# Apparatus for loss measurements under multidirectional and dc-bias flux in electrical steel laminations

W. Wang,[1)] A. Nysveen,[1)] and N. Magnusson[2)]

[1]*Department of Electric Power Engineering, Norwegian University of Science and Technology, NO-7491 Trondheim, Norway*

[2]*SINTEF Energy Research, NO-7465 Trondheim, Norway*

Conventional standardized power loss measurements for electric steels are performed at flux densities with a single sinusoidal and unidirectional excitation. However, the flux inside electrical steel laminations can deviate significantly from the standard condition and the loss is sensitive to such deviations of the flux in time and space. In this article, we describe the design and construction of an apparatus for loss measurements under two scenarios. 1) The main flux in the rolling direction is superimposed with flux in either the transverse or normal direction, while varying magnitude and phase angle between two fluxes. 2) The main flux having a dc-bias. The main flux in the rolling direction is generated in a square lamination frame by the current in excitation coils. The transverse and normal direction fluxes are generated by the current in auxiliary excitation coils wound around powder cores. The dc-bias flux is created either by an ac current with a small dc offset in the excitation coils or by a separate coil excited by dc current. We implement and compare the two dc-bias methods and discuss the commons and differences. Finally, we present experimental results showing the possibilities for loss measurements under the combined action of magnetic flux in different directions and under dc-bias.

## I. INTRODUCTION

Variable power production and load, due to e.g. wind and solar energy and charging of electrical vehicles, lead to new load patterns for power equipment, where the acceptance of short-time overloads can reduce the need for new investments. Also, the effect of geomagnetically induced currents (GICs) is a concern for network owners. These considerations lead to an increased importance of the loss in power equipment operating outside its design specifications. In transformers and rotational machines, the laminated iron cores are, in addition to the main flux following the direction of the core, exposed to magnetic leakage flux, which can be significant at high loads. In power transformers, the leakage flux enters the laminated core from different directions (see the flux lines entering the core in Fig. 1(a) and the definition of flux directions in Fig. 1(b)), leading to additional power loss in the laminations close to the windings. Depending on the orientation of the leakage flux relative the lamination, different loss mechanisms dominate the additional loss.

- Flux configuration 1: On the limb surface of the magnetic core, the leakage flux normal to the plane (ND) of the lamination induces eddy currents and thereby generates eddy current loss[1-3].
- Flux configuration 2: Under the yoke of the core, the leakage flux enters the core perpendicular to the rolling direction in the plane of the lamination (transverse direction, TD). Due to the thin laminations, the eddy currents induced by

the flux become small and the power loss is dominated by hysteresis loss. In many cases, the transverse leakage flux and the main flux are not in phase. The total magnetic field then becomes rotating and the power loss is associated with rotational hysteresis loss[4-7].

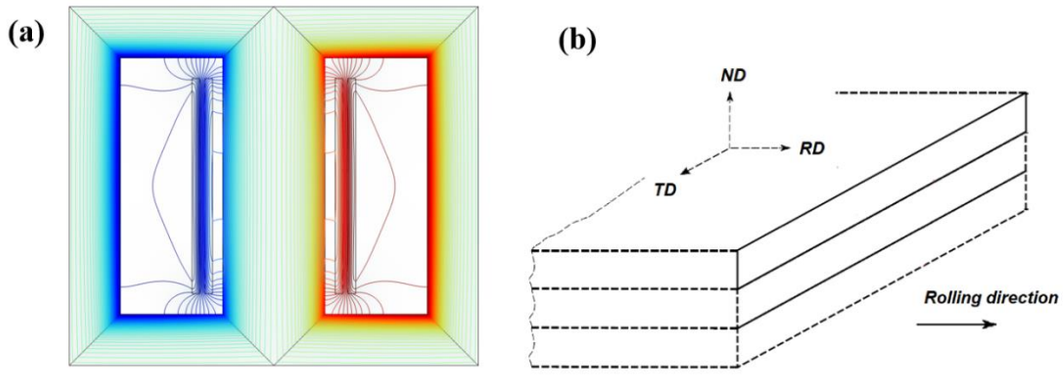


FIG. 1. (a) Flux distribution of a single-phase transformer obtained by a numerical simulation. The transformer shown is operating under resistive load. The flux distribution is presented at the time instant when the leakage flux density is at its maximum (i.e. the load current is at its peak and the main flux is at its zero crossing). (b) Definition of the flux directions in the grain-oriented steel laminations. RD: rolling direction; ND: normal direction; TD: transverse direction.

The strong anisotropy of the lamination structure[8] as well as the magnetic anisotropy of grain-oriented (GO) steel, prevent the incident flux to cross many of the lamination layers or reach far into the core in the transverse direction. Instead, the penetrated flux tends to close its loop on the surface layers of the lamination or along the edge of the lamination plane (see the flux line concentration and flux density distribution inside the core in Fig. 1(a)). Consequently, the surface layers and edges of the lamination are prone to be saturated, even when the incident leakage flux density is well below the saturation flux density of the steel, resulting in that the leakage flux becomes important also at relatively small amplitudes. Furthermore, the phase angle between the main flux and the leakage flux may play an important role for the loss, since eddy current loss and hysteresis loss are sensitive to both magnitude and the variation in time of the magnetic flux density.

The power loss in lamination cores is also sensitive to the dc-bias of the main flux[9-11]. Geomagnetic disturbances[12-14] can lead to GIC events where a dc current generates a dc-bias of the main field (and the same may occur due to power converter cross-modulation[15-16]). Dc magnetization leads to half-cycle saturation of the core in power transformers. This may result in harmonic pollution, reactive power consumption[14] and transformer over-heating[17].

Various power loss measurement apparatuses for magnetic materials have been proposed, which can be categorized into wattmetric[18-19], mechanical type[20] (torque magnetometers), thermometric[21-22], and fieldmetric[23-24]. The Epstein Frame[18] and the Single Sheet Tester (SST)[19] methods are the two standardized methods for measurements of the magnetic properties of electrical steel sheets, both based on the wattmeter method. The Epstein Frame consists of four coils into which strips to be tested are

inserted and assembled in a square. The losses are calculated from the current of the primary winding and the voltage of the secondary winding. In the single sheet tester, the sheet specimen is placed inside two windings (also here the primary winding yields the current and the secondary winding the voltage for the loss calculation) between a double-C laminated yoke[19]. In spite of the simplicity and applicability of the SST method, the Epstein method is at present still regarded as the sole reference method for the determination of the material quality[25]. The fieldmetric methods, while not yet standardized, are becoming widely used in rotational loss measurements, where 2-dimensional SST with various yoke configurations have been developed[23,26-27]. However, due to the limited area of uniform magnetization (comparable with the grain size of the material), the measurement does not allow for averaging of the properties over a large volume[4].

In both standardized methods (Epstein Frame and SST), the power loss is determined for flux densities with a single sinusoidal and unidirectional excitation. To meet the increasing importance of studying the loss in electrical sheets with the combined action of main flux and either leakage flux (including different phase shifts) or dc-bias flux, we have developed a measurement system based on the wattmeter method and the basic Epstein Frame geometry. The system is designed to characterize the power loss due to ac magnetic flux densities in RD combined either with dc-bias flux densities in the same direction or with flux densities in the TD direction. Additionally, the system allows for a replica of the actual leakage configurations in the laminated core for qualitative studies of the associated losses.

This paper is organized as follows. The loss components are introduced in Sec. II. The measurement principle is described in Sec. III, along with the equivalent circuit element models. The apparatus design is presented in Sec. IV, with details on construction of the lamination sample frame and the excitation systems. In Section V, the experimental results demonstrating the capability of the system are presented. Finally, a summary of the results is given together with the conclusions in Sec. VI.

## II. LOSS COMPONETS IN ELECTRICAL STEELS

Magnetic loss can be conceptually separated into eddy current loss, hysteresis loss and excess loss[28]. Eddy current loss and hysteresis losses arise due to successive reversal of magnetization in the iron core. The difference between the measured and calculated losses (eddy current and hysteresis loss) has been referred to as the anomalous loss (or excess loss)[29]. Regardless of this discrepancy, the two-component approach (eddy current and hysteresis loss) is still widely used, owing to its simplicity[4].

Eddy current loss ($P_e$), has its origin in induced voltages in the laminations in response to a sinusoidal magnetic flux in the lamination plane. Since the thickness of the sheet is much smaller than the skin depth power frequency, the eddy current loss can be expressed as[29]:

$$P_e = k_e f^2 t^2 B_{peak}^2 \quad (1)$$

where $k_e$ is a material dependent constant, $f$ [Hz] is the frequency of the magnetization, $t$ [m] is the thickness of individual sheets, and $B_{peak}$ [T] is the flux density. However, the relationship (1) can be largely violated when the flux is not oriented along the lamination plane. This is the case, for instance, when the leakage flux is normal to the lamination plane[1].

Hysteresis loss is caused by the irreversible domain wall movement and magnetization rotation within the domains in the magnetic material in response to a variable magnetic flux. Hysteresis loss is proportional to the enclosed area of the *B-H* curve (the hysteresis loop) under quasi-static alternating magnetization[29]:

$$P_h = k_h f B_{peak}^n \tag{2}$$

where $k_h$ is a material dependent constant, $B_{peak}$ [T] is the flux density, and $n$ is the Steinmetz constant having a value between 1.6 and 2.0 for hot rolled laminations and a value of more than 2.0 for cold rolled laminations[29]. However, when the flux has a dc-bias, the hysteresis loop becomes asymmetric. Depending on the level of the dc excitation, the loss feature can deviate significantly from the symmetric ac excitation[14] and, hence, the power loss then depends on both applied ac and dc flux.

When the material is subjected to a magnetic flux with its direction rotating in the plane of the lamination, the loss will be enhanced. As a comparison, the average power loss per unit mass for an alternating magnetization[5], $P_a$, and for rotational magnetization[30], $P_r$, are given by:

$$P_a = \frac{1}{\rho T}\int_0^T \left(\frac{dB_x}{dt}\cdot H_x\right) dt \tag{3a}$$

$$P_r = \frac{1}{\rho T}\int_0^T \left(\frac{dB_x}{dt}\cdot H_x + \frac{dB_y}{dt}\cdot H_y\right) dt \tag{3b}$$

where $\rho$ [kg/m$^3$] is the mass density of the material, $T$ [s] is the period of magnetization, and $B_{x(y)}$ [T], $H_{x(y)}$ [A/m] are the flux density and magnetic field strength in the x(y) direction.

## III. MEASUREMENT PRINCIPLE

The instrument serves two main purposes: 1. Material power loss characterization under multidirectional flux or dc-bias conditions. 2. Loss measurements with a replica of actual leakage flux configurations. The former requires homogenous field in a specified region and the measurement of power loss in such a region (isolating the contribution outside of the region) such that the specific loss can be obtained. In a unidirectional flux measurement such as an ac RD flux test or dc-bias test, this is straightforward since the flux is uniformly distributed in the whole sample and the loss contributed by the measurement device is negligible. The measurement principles of these types of tests are illustrated in III A, C. When multidirectional flux is considered, the flux-homogenous region shall be identified and the loss contribution outside the region as well as the contribution from the auxiliary devices shall be excluded. Such test is described in III. B (RD flux superimposed with TD flux).

The actual leakage flux configuration is far from homogenous as described in Section I. In a replica of such flux configurations, the inhomogeneous field should emulate real configurations. The measured loss variations give qualitative information of the behavior in real transformers. Since the loss is generated by an inhomogeneous field, the incremental power loss, instead of specific loss, is evaluated.

### A. Wattmeter-based loss measurement for RD flux

The wattmeter-based loss measurement equipment, such as the Epstein frame tester, comprises primary winding(s) used for setting up flux, secondary winding(s) used for voltage (flux) measurement and the specimen to be tested. The set-up forms an unloaded transformer. The schematic diagram for RD flux loss measurements is given in Fig. 2(a). The primary winding (to the left in Fig. 2(b)) is supplied with a sinusoidal current generating the magnetic flux. The current in the secondary winding has a component in phase with the flux, known as the magnetization current, and a component 90 degrees out of phase of the flux as a result of eddy current and hysteresis loss in the core[31]. The current in the primary coil and the voltage of the secondary coil are supplied to the wattmeter, generating the loss from the current and voltage components in phase with each other. If the sample had no losses, the current and voltage would be 90 degrees out of phase. Also, the measurement disregards any power loss in the primary winding since the voltage drop of this winding is not measured[4]. In the physical realization (Fig. 2(b)), the primary windings and the secondary windings form concentric windings, where the primary windings are located on the outside of the secondary winding. The individual primary windings as well as the individual secondary windings are connected in series.

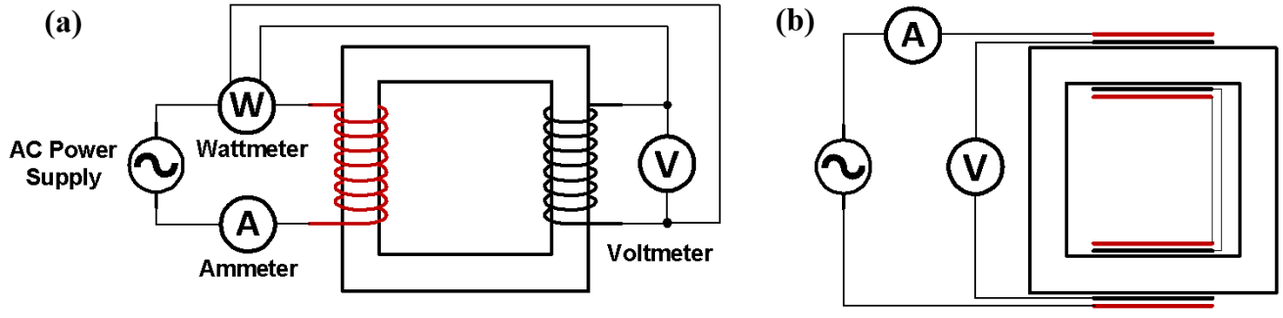


FIG. 2. The principle of wattmeter-based RD loss measurement (a) and the schematic diagram demonstrating the physical realization (b). The measurement system consists of primary winding, secondary winding and the specimen (core). The current from the primary side and the voltage from the secondary side are incorporated in the wattmeter. In the physical realization (b), the primary windings (red) are located on the outside of the secondary windings (black).

The secondary voltage $V_{2,rms}$ is calculated from the desired value of magnetic polarization (which is practically equal to the magnetic flux density) by:

$$V_{2,rms} = \sqrt{2}\pi f N_2 A B_{peak} \tag{4}$$

where $N_2$ is the total number of turns of the secondary winding, $A$ [m$^2$] is the cross-sectional area of the corresponding core. Since the internal impedance of the voltage measurement is high, the voltage measurement is practically equal to the induced voltage and the power consumed by the instruments in the secondary circuit is negligible. In a measurement, the power supply is tuned until the secondary voltage of the laminated frame reaches the values calculated from the designated flux densities. Then the power losses from the power analyzer are recorded. The specific loss $P_s$ [W/kg] is calculated by:

$$P_s = \frac{N_1}{N_2}\frac{P_m}{m} \tag{5}$$

where $P_m$ [W] is the reading from wattmeter and $m$ [kg] is the mass of the sample.

### B. Loss due to RD flux superimposed with TD flux

A schematic diagram for measurement of the loss due to the combined action of RD and TD flux is given in Fig. 3. The main (RD) flux circulating the frame is generated by an ac power supply in the same way as in Section IIIA. To create TD flux in the lamination, a notched ring core (NRC) is introduced. As for the main frame, the NRC is wounded with primary and secondary windings, forming a concentric winding. The primary windings of the main frame and the NRC are excited by independent voltage supplies such that the phase shift between the two sources can be adjusted flexibly. The NRC is clamped one branch of the lamination where the incident flux is forced to cross the lamination plane transverse to the rolling direction.

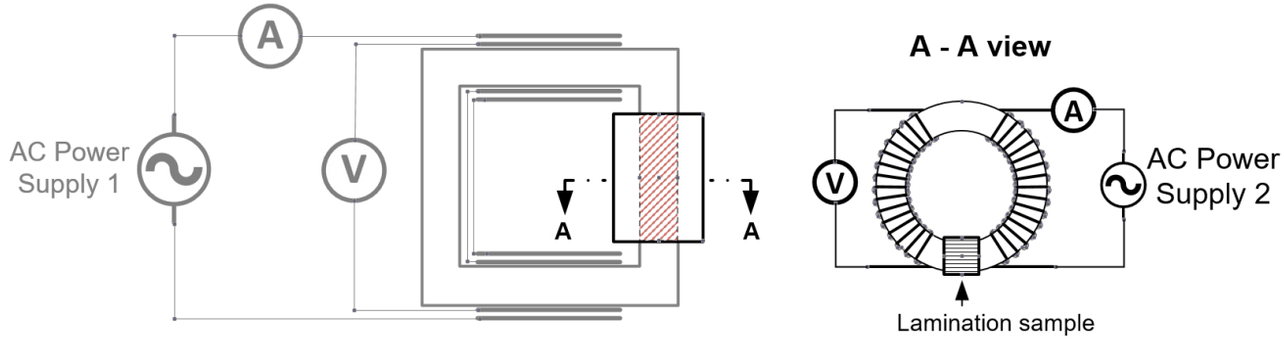


FIG. 3. Schematic diagram of the loss measurement system with RD flux superimposed with TD flux. The grey part is identical with Fig. 2. The ac power supply 2 connects to the primary winding wrapping around the NRC and supplies TD flux. The NRC is clamped on one branch of the lamination such that the transverse flux crosses the lamination plane (red area).

The secondary winding of the NRC is used as a voltage pick-up coil. Based on equation (4), the voltage of the NRC is set to obtain the desired values of the magnetic flux densities. In a measurement, two power supplies are tuned until the secondary voltages of the lamination frame and the NRC reach the values calculated from the designated flux densities. Then the power

losses from the power analyzer are recorded. The total net loss $P_{net}$ of the test specimen is a sum of the loss measured by the two coil systems withdrawing the power loss in the NRC:

$$P_{net} = \frac{N_1}{N_2}\tilde{P}_m + \frac{N_1^a}{N_2^a}\tilde{P}_m^a - P_{pow} \tag{6}$$

where $\tilde{P}_m$ [W] and $\tilde{P}_m^a$ [W] are the losses obtained from the wattmeter of the main excitation system (supplies the RD flux) and the NRC excitation system (supplies the TD flux) respectively. The measurement is performed when both the lamination frame and the NRC are excited simultaneously. $P_{pow}$ [W] is the power loss of the NRC, which needs to be measured according to the IEC standard[32] under specified flux densities and frequency prior to fabrication. Furthermore, the specific loss of the effective volume involved in the RD flux superimposed with the TD flux, can be defined:

$$P_s = \frac{1}{m_e}\left(P_{net} - P_{ineff}\right) \tag{7}$$

where $m_e$ [kg] is the mass of the effective volume involved in multidirectional flux. $P_{ineff}$ [W] is the loss of the ineffective volume that is not exposed to the TD flux. Since only unidirectional flux is involved in this region. The value of $P_{ineff}$ can be obtained from the ac RD flux measurement.

The transverse flux distribution is less homogeneous at the ends of the frame volume (measurement volume) covered by the NRC, as some of the TD flux passes outside the measurement volume (and thereby lower the flux inside the measurement volume), see Fig. 4. To counteract the effect of the flux inhomogeneity, we have assembled two NRCs with different dimensions, one NCR comprising 3 units of the rings and the other 5 units. The loss contributed by the inhomogeneity is then minimized by subtracting the measurement using the 3-unit NCR from the measurement using the 5-unit NCR. The difference between the two measurements is then the contribution from the TD flux area of two units in the middle where the flux is practically homogenous (effective volume). Therefore, the measurement quantities $P_m^a$ [W] and $\tilde{P}_m$ [W] in (6) are replaced with:

$$\begin{cases} P_m^a = P_{m5}^a - P_{m3}^a \\ \tilde{P}_m = \tilde{P}_{m5} - \tilde{P}_{m3} \\ \tilde{P}_m^a = \tilde{P}_{m5}^a - \tilde{P}_{m3}^a \end{cases} \tag{8}$$

where the subscripts 3 and 5 indicate the measurement with 3-unit core and 5-unit core, respectively.

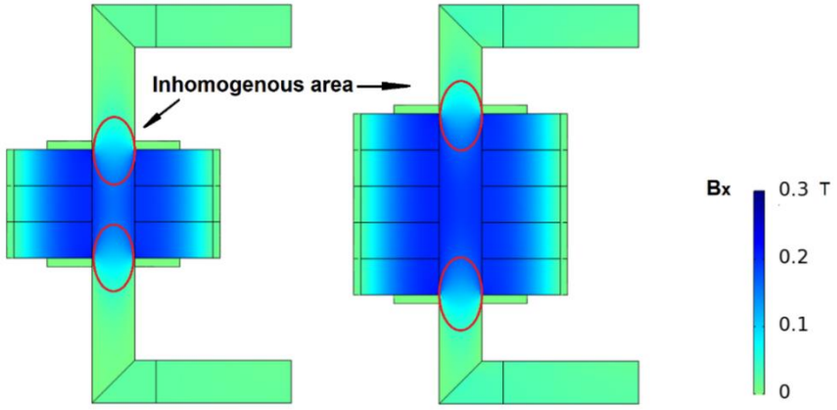


FIG. 4. Example of the transverse flux distribution (flux density in the horizontal direction, $B_x$) in the lamination. The end (inhomogeneity) effect is cancelled out by subtracting the measurement of 3-unit core from the measurement of 5-unit core.

### C. Loss due to RD flux with dc-bias

The schematic diagram of the loss measurement system under dc-bias is given in Fig. 5. Two methods of introducing dc-bias in the flux can be implemented. In the first method, we add the voltage offset directly from the power supply (Fig. 5(a)). In a measurement, the ac voltage source is tuned until the induced secondary voltage of the lamination frame reaches the value calculated from the designated flux density, and the dc voltage offset is tuned until the dc component of the primary current reaches the designated value. Then the power losses from the power analyzer are recorded. The advantages of this approach are its simplicity and that it is similar to the real GIC scenario. The disadvantage is the need for delicate tuning of the dc voltage offset (dc-bias is order of magnitude smaller than the ac signal due to the low resistance and the high number of turns of the primary winding). In the second method, we introduce a dc flux using a separate excitation coil (Fig. 5(b)), which enables an easy tuning since the dc flux is excited separately. The ac voltage source is tuned in the same way as in method 1, whereas the dc current (corresponding to dc MMF) is directly tuned to the designated value. However, a large inductance is required to smooth the current induced by the coupling system. In both methods, the loss measurement is straightforward and the equation (5) is used to calculate the specific power loss.

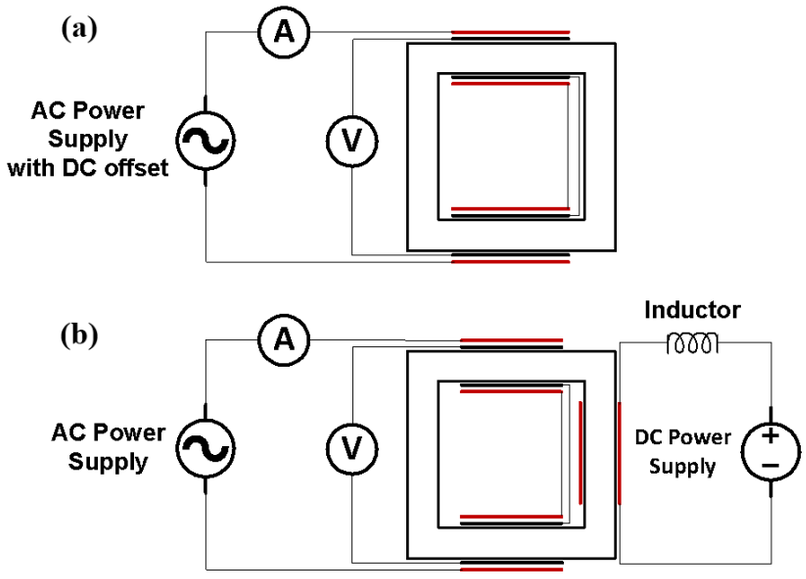


FIG. 5. Schematic diagram of the loss measurement system under dc-bias. (a) The excitation voltage applied on the primary coil has a small dc-bias. (b) The dc-bias is introduced by a separate coil (on the right) connected to a dc power supply and an inductor for current smoothing.

### D. Replica of actual leakage flux configuration

As described in Section I, we categorize the leakage flux into two typical configurations in actual situations. That is, depending on the position exposed, the leakage flux can either be normal or transverse to the core lamination. In either case, inside the lamination the penetrated flux turns to be parallel to the RD and returns to the leakage channel on the same side of the lamination plane. Therefore, the power loss is practically determined by the incident leakage flux (either TD or ND) combined with the penetrated flux parallel to RD. To reflect these actual flux configurations, a C-shaped core (CSC) is utilized to produce an 'artificial leakage flux'. Instead of enforcing the flux crossing the lamination plane as in Section IIIB, the CSC imposes and absorbs the flux on the same side of the lamination. We mount the CSC in two positions, so that the incident flux can enter either transverse (TD) or normal (ND) to the lamination plane, whereas the penetrated flux along the edge or surface is parallel to the RD.

Schematic diagrams for measurements representing actual leakage flux configurations are given in Fig. 6. As for the NRC, the CSC has primary and secondary windings. The primary windings of the CSC and the main frame are excited by independent voltage supplies such that their phase angle can be adjusted flexibly, whereas the secondary winding of the CSC is used as voltage pick-up coil. In configuration Fig. 6(a), the CSC is mounted on the side of the lamination where the incident flux is in the TD, whereas in configuration Fig. 6(b) the CSC is mounted on top of the lamination where the incident flux is in the ND. In a measurement, two power supplies are tuned until the induced secondary voltages of the lamination frame and the CSC reach the values calculated from the designated flux densities. Then the power losses from the power analyzer are recorded.

To investigate the variation in loss due to an added flux , the concept of incremental loss, $P_{incr}$ [W], is introduced, which is the difference between $P_{net}$ (under superimposed flux) and the arithmetic sum of the loss measured with the individual excitation systems alone (under unidirectional flux).

$$\begin{aligned} P_{incr} &= P_{net} - \left(\frac{N_1}{N_2}P_m + \frac{N_1^a}{N_2^a}P_m^a - P_{pow}\right) \\ &= \frac{N_1}{N_2}\left(\tilde{P}_m - P_m\right) + \frac{N_1^a}{N_2^a}\left(\tilde{P}_m^a - P_m^a\right) \end{aligned} \tag{9}$$

where $P_m$ [W] and $P_m^a$ [W] are the losses of the main excitation system and the auxiliary excitation system measured individually. Note that $\tilde{P}_m$ *is* different from $P_m$ since it changes with the applied flux.

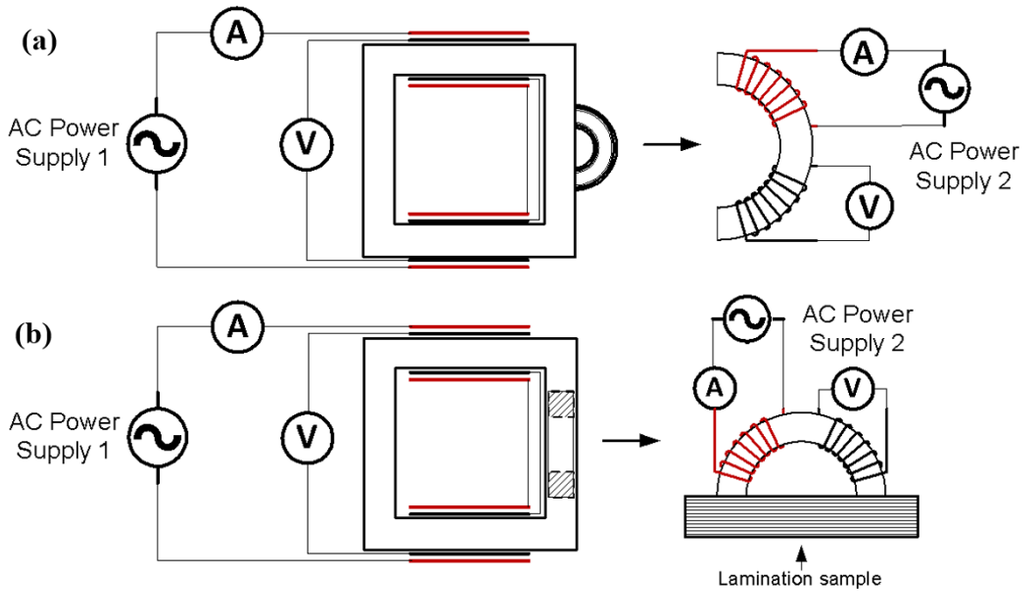


FIG. 6. Schematic diagram of the loss measurement system representing the actual leakage flux configurations. The AC power supply 1 connects to the primary windings wrapping around the square frame and supplies main flux. The AC power supply 2 connects to the winding wrapping around the CSC. In the configuration (a), the CSC is mounted on the side of the lamination and supplies TD flux to the lamination. In the configuration (b), the C shaped core is mounted on the surface of the lamination and supplies ND flux to the lamination.

Note that the replica of the leakage flux configuration only yields qualitative results and cannot directly be used for material characterization since the loss depend on the geometry chosen (e.g. size of lamination frame and cross-section of CSC).

## IV. LOSS MEASUREMENT SYSTEM

### A. Lamination sample frame

The strips to be tested (cold rolled grain oriented electric steel, Grade 30P120, Standard[33] JIS 2553, Japan) were cut along the rolling direction (with angle tolerance of 1°), where the edge of the sheet defined the reference direction, and were then assembled into a frame. The frame was similar to an Epstein frame, with some important distinctions:

- The strips were assembled in a square with mitered joints (see Fig. 7), instead of double-lapped joints used in the Epstein frame. The angle of overlap was 45°. The mitered joints were preferred for two reasons: 1. the loss in the corner joints was minimized since the flux in the joint became parallel to the of grain orientation[29]; 2. the filling factor became close to that of a real transformer.
- The lamination frame consisted of two coil groups positioned on the opposite sides of the frame (see Fig. 7). Each coil group had two concentric windings: an outermost primary winding (magnetizing winding), and an innermost secondary winding (voltage pick-up winding). The number of turns was selected to adapt to the power source, the measuring equipment and the frequency.
- The overall thickness of the lamination stack was 30 mm (larger than the Epstein frame sample) to match the thickness of the powder core in the auxiliary excitation system. Additionally, the chosen volume secured that the imposed flux channel was not limited by the thickness of the sheets.

The detailed design parameters are listed in Table I.

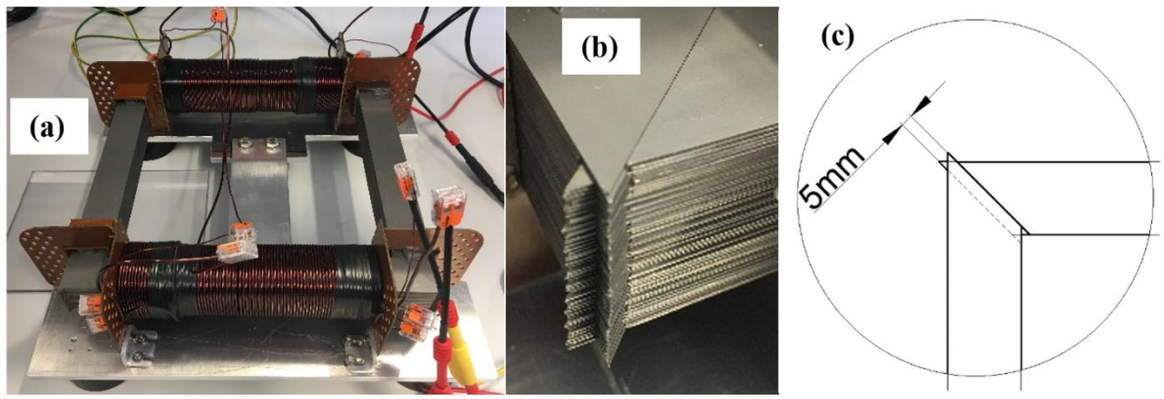


FIG. 7. The frame of the lamination sample with coils. (a) The lamination frame and the coils formed the magnetic circuit. The frame comprised a sheet lamination with 103 layers, 30 mm in height. The individual primary and secondary windings of the two coils were connected in series. (b)(c) The mitered joints have a 5 mm offset and the angle of overlap was 45°.

The laminated frame works as a no-load transformer, on which the maximum flux density applied is below the saturation point. Therefore, the power loss due to leakage flux from the frame is insignificant. In addition, metallic loops are avoided around the branch of the frame as it would lead to extra loss, which would influence the measurement results. The coils were fixed to insulating supports (inner width 31 mm) and an aluminum baseplate.

The complete frame had several mechanical clamps to avoid displacement of the laminations due to strong vibration caused by magnetostriction. Equation 4 implies that a proper definition of the cross-sectional area is crucial to obtain the actual flux

density. Considering that a large deviation of the individual sheet thickness from the nominal value, the statistically reliable effective cross-sectional area[18], *A*, was used:

$$A = \frac{m}{4l\rho} \tag{10}$$

where $m$ [kg] is the total mass of the test specimen, $l$ [m] is the length of a test specimen strip, and $\rho$ is the mass density (7.65 kg/dm$^3$ for 30P120[33]). The calculated filling factor was 0.968.

TABLE I. Parameters of the lamination sample frame and the coils.

| Parameters | Value | Unit |
|---|---|---|
| Total number of sheets | 4×103 | … |
| Total number of coils | 2 or 3[a] | … |
| Sheet width | 30 | mm |
| Sheet thickness | 0.30±0.03 | mm |
| Frame outer length | 280±0.5 | mm |
| Frame inner length | 220±0.5 | mm |
| Frame cross-section area | 900[b] | mm$^2$ |
| Effective frame cross-section area | 871 | mm$^2$ |
| Length of individual coils | 190 | mm |
| Number of turns, primary coil | 2×100 | … |
| Number of turns, secondary coil | 2×100 | … |
| Primary coil wire diameter | 2 | mm |
| Secondary coil wire diameter | 1 | mm |

[a]3 is the number of coils used for dc-bias test with separate excitation.
[b]900 mm$^2$ is the geometric cross-sectional area.

### B. NRCs and their excitation systems

The NRCs and the excitation coil systems are shown in Fig. 8. High Flux (Magnetics©) powder cores, offering much higher saturation flux density (1.5 T) than ferrites and lower loss than powder iron cores, were used as the starting material. For experiments where low flux densities (< 0.5 T) are of interest, a ferrite core can be an alternative to reduce core loss. The 30 mm opening (the notch) for the frame was machined from each 25.4 mm wide ring core. The two NRCs used were assembled using 3 and 5 units of powder rings, yielding total widths of 76.2 and 127 mm, respectively. The excitation and voltage pick-up coils were wound around the NRCs. The detailed design parameters are listed in Table II. The attainable flux densities (peak values), the corresponding applied voltages and the excitation currents are listed in Table III. The loss in the lamination frame and in the NRCs must be pre-measured individually over the span of flux densities used in the experiments.

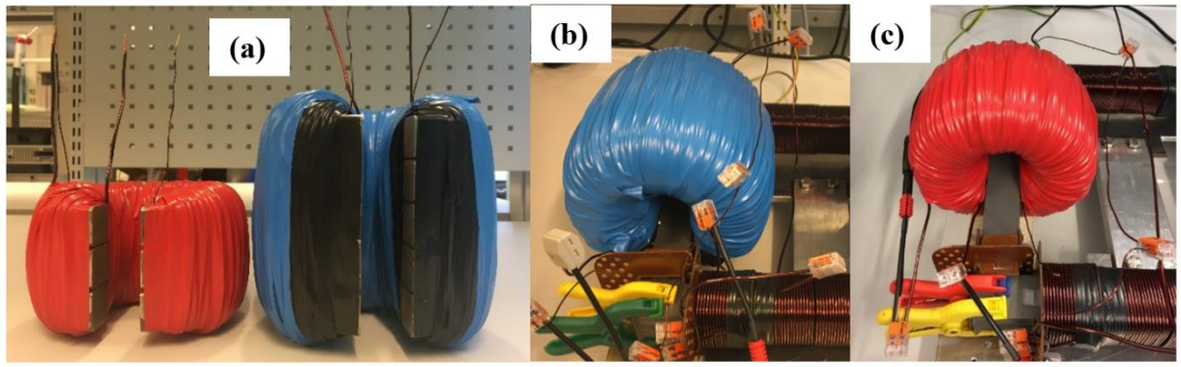


FIG. 8. NRCs and the excitation systems. (a): Notched ring cores (NRCs) are made of 3 units and 5 units of 25.4 mm wide powder rings with 30 mm slots. NRCs of 5 units (b) and 3 units (c) are mounted on the middle of the lamination branch.

TABLE II. Parameters of the NRCs and the excitation systems.

| Parameters | Value | Unit |
|---|---|---|
| Relative permeability of the ring | 125 | … |
| Outer diameter of ring | 132.6 | mm |
| Inner diameter of ring | 78.6 | mm |
| Height of ring | 25.4 | mm |
| Cross-section area of ring | 678 | $mm^2$ |
| Total cross-section area, 3-unit NCR | 3×678 | $mm^2$ |
| Total cross-section area, 5-unit NCR | 5×678 | $mm^2$ |
| Number of turns, primary coil, 3-unit NCR | 200 | … |
| Number of turns, primary coil, 5-unit NCR | 350 | … |
| Number of turns, secondary coil, 3-unit NCR | 100 | … |
| Number of turns, secondary coil, 5-unit NCR | 100 | … |
| Primary coil diameter | 1.95 | mm |
| Secondary coil diameter | 0.8 | mm |

TABLE III. Flux density, voltage and excitation current ranges on the main and the NCR excitation systems at 50 Hz.

| Excitation coil | Flux density [T] | RMS voltage range [V] | Excitation current [A] |
|---|---|---|---|
| Lamination frame | 0 - 1.6 | 0 - 62 | 0 - 0.72 |
| NRC (3 unit) | 0 - 0.8 | 0 - 72 | 0 - 5.5 |
| NRC (5 unit) | 0 - 0.8 | 0 - 211 | 0 - 3.2 |

### C. CSC and its excitation system

Figure 9 shows the CSC with excitation and voltage pick-up coils. Since the permeability of the powder core is much lower than that of GO steel, the impact of the main flux on the powder core is negligible when the GO steel works in its linear region. In the measurement where the flux superimposition takes place, the permeability of the GO steel reduces considerably. Consequently, the stray flux from the frame can enter the auxiliary core and influence measured power loss. To avoid the measurement inaccuracy introduced by the flux interaction, 1 mm thick plastic spacers were used to magnetically insulate the

main frame flux from the saturated GO steels. The ring unit used in CSC was identical with the one in the NRC (see Table III). The coil parameters are listed in Table IV.

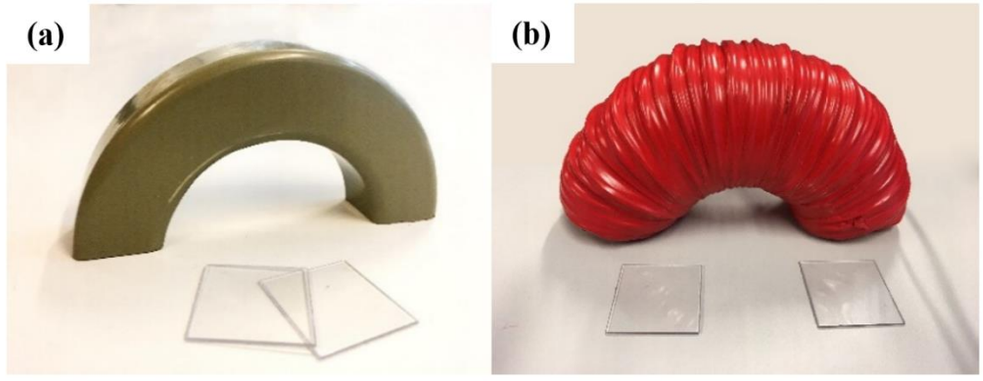


FIG. 9. CSC and the excitation system. (a) The C-shaped core (CSC) was made by a half ring unit. (b) The excitation and voltage pick-up coils were wound around the CSC. Plastic spacers were used to create air gaps.

TABLE IV. Parameters of the CSCs and the auxiliary excitation systems.

| Parameters | Value | Unit |
|---|---|---|
| Number of turns, primary coil | 200 | … |
| Number of turns, secondary coil | 100 | … |
| Primary coil diameter | 1.95 | mm |
| Secondary coil diameter | 0.8 | mm |

The CSC was placed in the middle of one branch of the frame using mechanical clamps. There are two possible positions for the CSCs, as described in Fig. 6. To obtain incident flux in the normal direction, the CSC was placed on the plane of the lamination, see Fig. 10(a). With the CSC mounted on one side of the lamination, the incident flux entered the laminations in the transverse direction, see Fig. 10(b). The desired flux densities and the corresponding applied voltages and excitation currents are listed in Table V. The losses in the auxiliary excitation system were pre-measured under the same given flux.

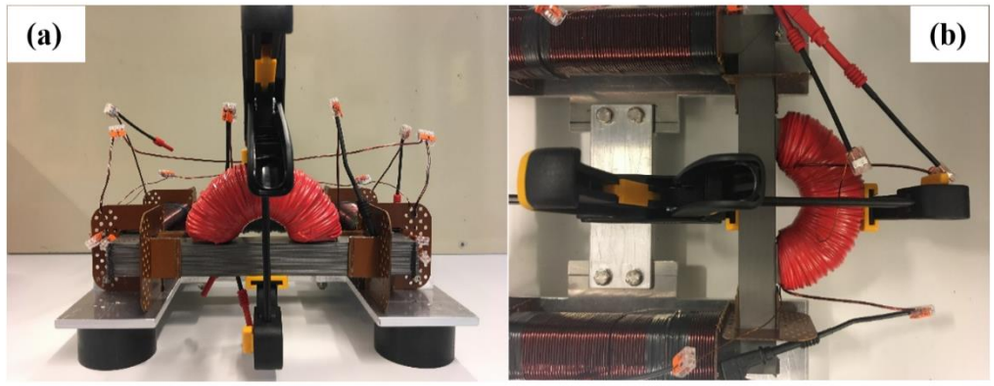


FIG. 10. The CSC was mounted on one branch of the lamination frame. (a) The CSC mounted on the plane of the lamination, yielding incident flux in the normal direction. (b) The CSC mounted on the side of the lamination, yielding incident flux in the transverse direction.

TABLE V. Flux density, voltage and excitation current ranges on the main and the CSC excitation systems at 50 Hz.

| Excitation coil | Flux density [T] | RMS voltage range [V] | Excitation current [A] |
|---|---|---|---|
| Lamination frame | 0 - 1.6 | 0 - 62 | 0 - 0.72 |
| CSC | 0 - 0.8[a] | 0 - 24 | 0 - 6.1 |

[a]0.8 T is the maximum flux density applied on the CSC, which is well below the saturation flux density of the powder core (High Flux Magnetics©). The tests were performed with flux densities where the distortion of the induced voltage waveform was low (THD<5%).

### D. Measurement instruments

The main measurement instruments were a power supply and a high precision power analyzer, see Fig. 11. The lamination frame was connected to the instruments according to the circuit diagrams described in Section III. The power supply used could provide independent voltage sources where the phase difference, frequency and magnitude between them were fully controllable. The current and voltage measurements were made by the power analyzer, where the power loss was obtained. Oscilloscope functions were embedded in both the power supply and the power analyzer such that the voltage, current waveforms and the phase difference could be verified and recorded online.


FIG. 11. Measurement instruments. The setup consisted of the lamination test sample (1), the power analyzer, YOKOGAWA WT3000 power analyzer (2) and the power supply, ITECH IT7627 High power programmable AC power supply (3).

Two distinct methods of introducing dc-bias were implemented according to Sec. IIIC. In the first method (Fig. 5 (a)), the resultant steady state dc current was determined by the dc voltage offset $V_{dc}$ [V] and dc resistance $R_{dc}$ [Ω] of the circuit. The definition is in line with the GIC definition[34].

$$I_{dc} = \frac{V_{dc}}{R_{dc}} \tag{11}$$

The reading of the power loss $P$, peak value $I_{peak}$ and dc component $I_{dc}$ [A] of the (magnetization) current were recorded from the power analyzer. The waveforms of the voltages and currents were saved to construct the magnetization curve.

In the second method, a separate excitation coil (Fig. 12) was used to introduce the dc flux. The turn number of the dc excitation coil (40 turns) was chosen based on the capacity of the measurement system and the power supply. With a high number of turns, the induced voltage on the dc excitation circuit becomes high, requiring a large inductance to smooth the current ripple. A lower number of turns demands a high dc current, which should be supplied by the dc power source and handled by the measurement instruments. A large inductance (600 mH was used in our test, giving approximately 3% current ripple) was used to smooth the induced current. The attainable ac flux densities (peak values), the corresponding voltages as well as the dc voltages and currents are listed in Table VI.

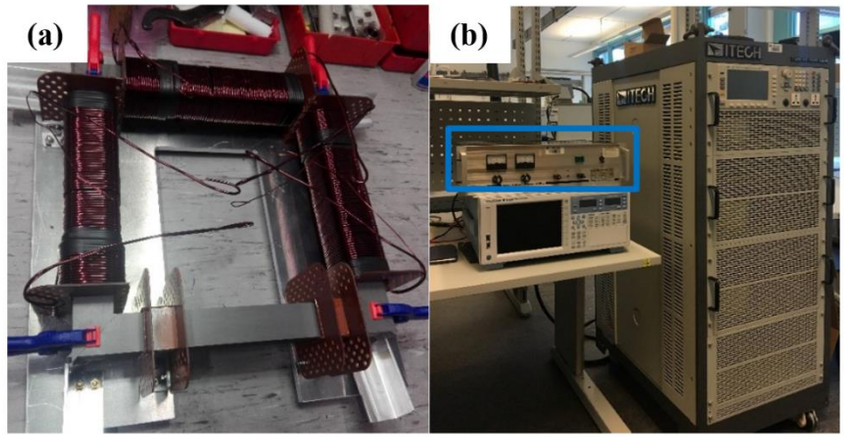


FIG. 12. Experimental setup for loss measurements under dc-bias. In method 2, a dc-bias was introduced by a separate coil excited by a dc power source. (a) The coil for dc excitation was added as a third winding on the upper branch in the figure. (b) The dc excitation coil was controlled by a separate dc power source.

TABLE VI. Voltage and current applied for loss measurement under dc-bias.

| Parameter | Range | Unit |
|---|---|---|
| Flux density | 0 - 1.6 | T |
| AC RMS voltage applied | 0 - 62 | V |
| DC voltage range, method 1 | 0 - 0.5 | V |
| DC current range, method 2 | 0 - 20 | A |

## V. MEASUREMENT EXAMPLES

### A. Loss measurement with RD flux superimposed with TD flux

Loss measurement results for the sample exposed to RD superimposed with TD flux of varying magnitudes are given in Fig. 13. For the entire TD flux density span, the difference in power loss between $B_{RD}$=1 T and $B_{RD}$=1.6 T is almost constant. Compared to the RD flux density, the TD flux has a major impact on the power loss, particularly when the TD flux density is high (≥0.4 T), whereas the phase angle has a lower impact on the power loss. Homogenous TD flux induces significantly higher

per unit loss than RD flux. However, the actual TD flux in the core is far from homogenous and confined within a small region, thus, the loss contribution is insignificant.

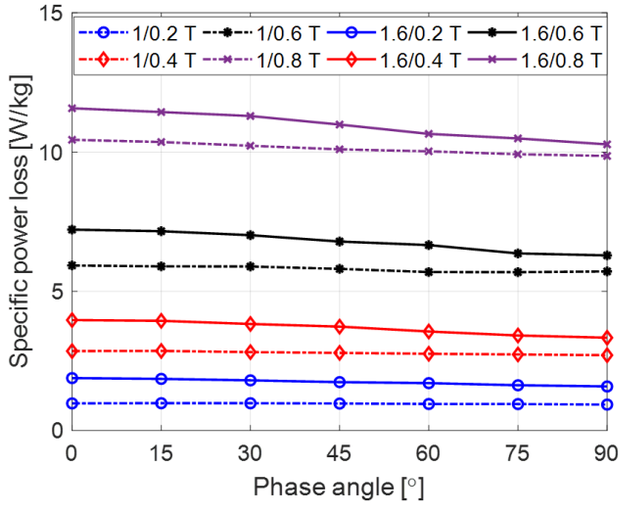


FIG. 13. Measured specific power loss versus phase angle in the region having RD flux superimposed with TD flux. RD flux densities were 1 T (dashed line) and 1.6 T (solid line). TD flux density varies from 0.2 T to 0.8 T.

### B. DC bias measurements

An example of the measurement of the *B-H* characteristics of the sample under different dc-bias levels is demonstrated in Fig. 14(a), using method 1. The comparison of the magnetization currents obtained from two methods is described in Fig. 14(b), and the corresponding frequency spectra are shown in Fig. 14(c). It is seen that the dc flux adds to the amplitude of the ac flux in one half-cycle and subtracts in the other half-cycle, resulting in half-cycle saturation.

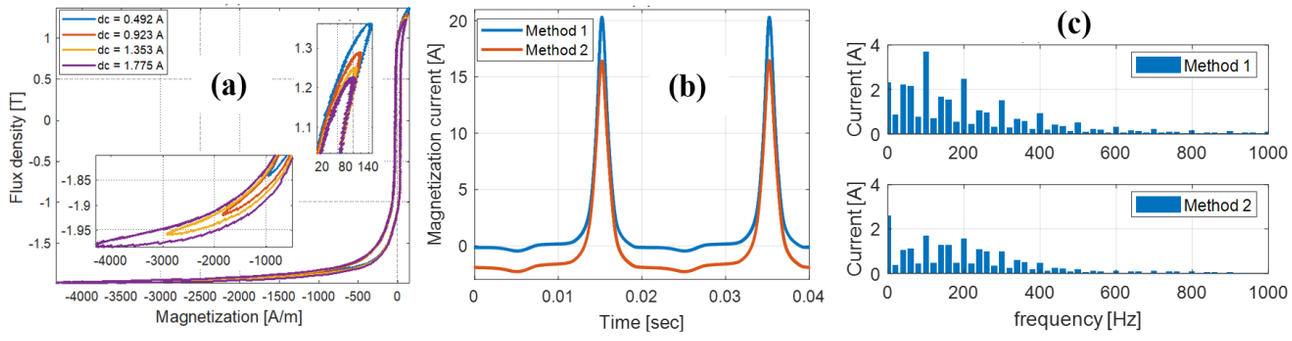


FIG. 14. Examples of loss measurements under dc-bias. (a) Magnetization characteristic (B-H curve) under four different dc-bias levels using method 1. (b) Comparison of magnetization currents at NI=355 A (the number of turns is implicitly accounted) using the two methods. (c) Comparison of the spectra of magnetization currents using the two methods.

The offset of the dc flux density depends on the magnitude of the dc current, the number of turns, and the reluctance of the flux path. The dc flux density cannot be measured by an inductive measurement method, and a direct method, using a Hall

effect sensor, is demanding, due to the difficulty of placing the sensor in the lamination. To overcome the problem, we adopted a comparative method to derive the flux offset indirectly. In this approach, we used the ac over-excitation test result as a reference, i.e. a $B$-$I_{peak}$ characteristic curve. $I_{peak}$ obtained from the dc-bias test was compared to the preserved $B$-$I_{peak}$ curve, where the maximum flux density $B_{max}$ was identified. Since the peak-to-peak flux density was obtained by the ac voltage source, the dc-bias was then calculated by

$$\Delta B = B_{max} - B_{ac} \tag{12}$$

where $B_{ac}$ corresponds to the applied ac voltage. The calculated offset flux densities corresponding to Fig. 14(a) were 0.236 T, 0.311 T, 0.349 T and 0.371 T, respectively.

The comparison of magnetization currents (Fig. 14(b)) shows the similarity in the magnetization current waveforms. The difference is, in method 2, that the average of the current $I(t)$ over a period $T$ should be zero, which gives the constraint:

$$\int_0^T I(t)\, dt = 0 \tag{13}$$

Despite the difference in spectra, the loss measured using the two methods are very similar, see Fig. 15. The small difference can be attributed to the ripple in the dc current using method 2. Another important observation is that the saturation effect of the power loss occurring as the dc magnetomotive force (MMF) increases. The moderate change of the hysteresis loss can be explained by the variation of the hysteresis loop in Fig. 14(a). Due to the dc offset of the flux, the area of the hysteresis loop increases in one half-cycle and reduces in the other half-cycle. As dc MMF further increases, the peak flux exceeds the saturation point in one half-cycle. Consequently, the increase rate of the hysteresis loop area starts to slow down in one half-cycle, while the decrease rate of the area is maintained in the other half-cycle. In combination, the total hysteresis loss asymptotically approaches a maximum value with increasing dc MMF.

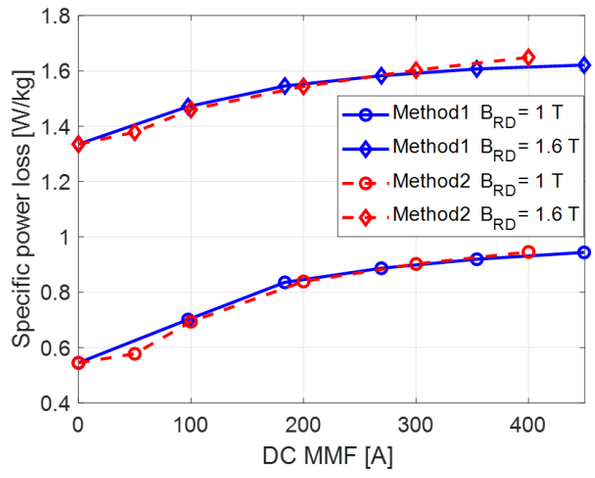


FIG. 15. Measured specific power loss versus dc magnetomotive force (dc-bias level) with the low ac flux density (1 T) and the nominal flux density (1.6 T). The dc magnetomotive force (MMF) is varied from 0 to 450 A (the number of turns is implicitly accounted).

Due to larger values of the magnetization current in method 1, the winding losses and stray losses (associated with the magnetic current) becomes higher when using method 1 than when using method 2. Therefore, to be conservative, the method 1 is recommended for transformer dc-bias tests.

### C. Replicas of actual leakage flux configuration

Measurement results with replica of actual leakage flux configurations are demonstrated in Fig. 16. In Fig. 16(a), the power loss increases dramatically with increasing ND flux density and frequency. The incremental loss due to RD flux superimposed with TD flux is demonstrated in Fig. 16(b). We can observe a significant increase in power loss with decreasing phase angle between the RD and TD flux. This increment is due to that the sum of RD flux generated by the main field coil and the RD flux coming from the TD flux (as it flows in the RD direction to close the magnetic loop of the C-core) at small phase angles results in enhanced RD flux density amplitudes and thereby increased loss. Hence, the conventional no-load test under-estimates the losses under inductive loading (small phase angle). The small discrepancy at 90° phase angle implies that the conventional no-load test gives a good estimation on overall core loss in normal operation.

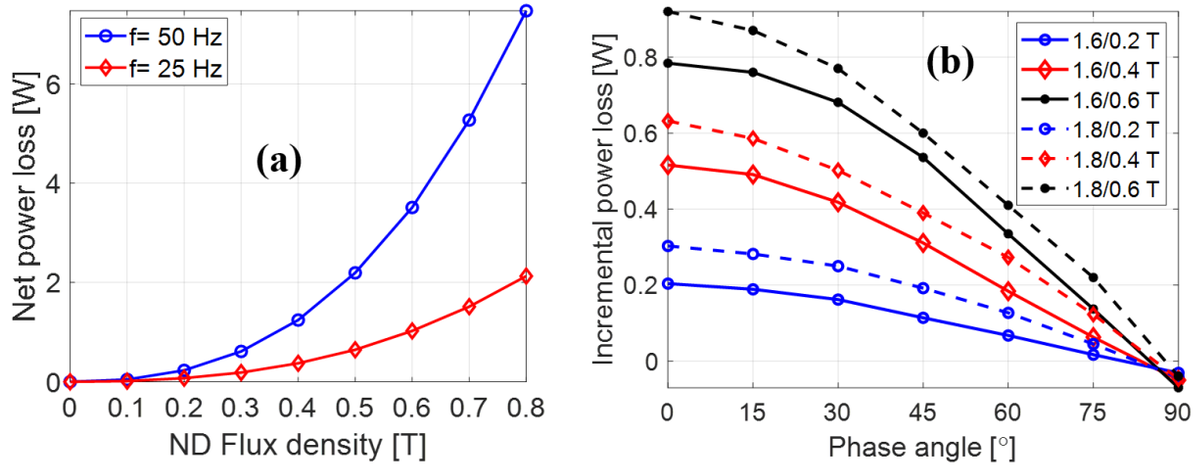


FIG. 16. Examples of loss measurements with the replicas of actual leakage flux configurations. (a) Net power loss in the lamination versus flux density in the normal direction (without RD flux) at 25 and 50 Hz. (b) Incremental power loss versus phase angle in the transverse direction at 50 Hz. The RD flux densities are 1.6 T and 1.8 T, and the TD flux density varies from 0.2 T to 0.6 T.

As illustrated in Sections I and III. D, the leakage flux enters the core normal or transverse to the lamination plane. Initially, the flux is constrained within a small depth where it maintains its orientation inside the core, we call it the local zone. Inside the local zone, the induced loss due to ND flux is dominated by the eddy current loss, whereas the loss due to TD flux is dominated by the rotational power loss (when the TD flux and the RD flux are not in phase). Outside the local zone, the penetrated flux changes direction, turn to be parallel to the RD and eventually return to the leakage channel on the same side

of the lamination plane. Here the flux follows the edge of the core window and has a significantly larger influence area, which forms the global zone.

As the power losses measured under actual leakage flux configurations are combinations of RD flux and ND (or TD) flux, it consists of loss contributed from both the local zone and the global zone. Flux superimposition not only increases the resultant magnitude of the flux density, but also extends the influence region due to flux saturation. Figure. 16(b) reveals that both the magnitudes of the RD flux and ND (or TD) flux and the phase angle between them plays a crucial role in power loss enhancement, and the incremental loss predominantly takes place in the global zone. A small phase difference results in a larger increase of the resultant flux density and thereby a lager incremental loss, whereas the resultant flux density due to a 90-degree phase difference has a negligible increase in magnitude.

## VI. SUMMARY AND CONCLUSIONS

In this paper, the detailed design of an apparatus for measurement of losses in electrical steel laminations under multidirectional and dc-bias flux has been presented. Experimental measurements demonstrate the apparatus' ability to provide loss measurements in a large range of flux densities and orientations important for studying iron core losses in e.g. transformers under saturation.

The loss measurement system and measurement method could complement existing standardized tests (Epstein testing and SST) in characterizing the losses influenced by leakage flux and flux offset under various operation conditions, and serve as a guide to design engineers regarding the loss distribution and potential local (or global) heat enhancement generated by the leakage flux and flux offset.

## ACKNOWLEDGEMENT

This work was performed as a part of the project "Thermal Modelling of Transformers" (project number: 255178) funded by the Research Council of Norway, Statnett, Hafslund and Lyse Nett.

## DATA AVAILABILITY STATEMENT

The data that support the findings of this study are available from the corresponding author upon reasonable request.

## REFERENCE

[1]T. Booth and H. Pfützner, J. Magn. Magn. Mater., 133, 183-186 (1994).
[2]N. Hihat, J. P. Lecointe, S. Duchesne, E. Napieralska and T. Belgrand, Sensors 10, 9053-9064 (2010).
[3]T. Yagisawa, Y. Takekoshi and S. Wada, J. Magn. Magn. Mater., 26, 340-342 (1982).
[4]S. Zurek, *Characterisation of Soft Magnetic Materials Under Rotational Magnetisation*, 1st ed. (CRC Press, London, 2018).

[5]H. Pfützner, IEEE Trans. Magn., 30(5), 340-342 (1994).
[6]L. R. Dupre, F. Fiorillo, C. Appino, A. M. Rietto and J. Melkebeek, J. Appl. Phys., 87(9), 6511-6513 (2000).
[7]T. Kochmann, J. Magn. Magn. Mater., 160, 145-146 (1996).
[8]J. Wang, H. Lin, Y. Huang and X. Sun, IEEE Trans. Magn., 47(5), 1378-1381 (2011).
[9]X. Zhao, L. Li, J. Lu, Z. Cheng and T. Lu, IEEE Trans. Magn., 48(2), 747-750 (2012).
[10]J. G. Kappenman and V. D. Albertson, IEEE Spec., 27(3), 27-33 (1990).
[11]G. Ma, L. Cheng, L. Lu, F. Yang, X. Chen and C. Zhu, J. Magn. Magn. Mater., 426, 575-579 (2017).
[12]P. Price, IEEE Trans. Pow. Deli., 17(4), 1002-1008 (2002).
[13]R. Pirjola, IEEE Trans. Plasma Sci., 28(6), 1867-1873 (2000).
[14]R. Girgis and C. D. Ko, IEEE Trans. Pow. Deli., 7(2), 699-705 (1992).
[15]Y. Jiang and A. Ekström, IEEE Trans. Pow. Elec., 12(2), 287-293(1997).
[16]E. V. Larsen, R. A. Walling and C. J. Bridenbaugh, IEEE Trans. Pow. Deli., 4(1), 667-673 (1989).
[17]H. Tay and G. W. Swift, IEEE Trans. Pow. Appl. Syst. 104(1), 212-219. (1985).
[18]IEC 60404-2: 2008, *Magnetic Materials-Part 2: Methods of Measurement of the Magnetic Properties of Electrical Steel Strip and Sheet by Means of an Epstein Frame*.
[19]IEC 60404-3: 2009, *Magnetic materials-Part 3: Methods of Measurement of the Magnetic Properties of Electrical Steel Strip and Sheet by Means of a Single Sheet Tester*.
[20]F. Brailford, J. IEE. 95, 175-177 (1948).
[21]F. Fiorillo, et al., *Proceedings of the 1st 1&2DM Workshop*, Braunschweig, Germany, p.162, 1992.
[22]C. Ragusa, et al., J. Magn. Magn. Mater., 320(20), 623-626 (2008).
[23]Y. Enokizono, T. Suzuki, J. Sievert and J. Xu, IEEE Trans. Magn, 26(5), 2562-2564 (1990).
[24]V. Gorican, et al., *Proceedings of the 6th 1&2DM Workshop*, Bad Gastein, Austria, p.66, 2000.
[25]C. Appino, E. Ferrara, F. Fiorillo, L. Rocchino, *et al.*, J. Appl. Elec. and Mech., 48, 123-133 (2015).
[26]W. Brix, K. Hempel and F. Schulte, IEEE Trans. Magn., 20(5), 1708-1710 (1984).
[27]T. Nakata, N. Takahashi, K. Fujiwara and M. Nakano, IEEE Trans. Magn., 29(6), 3544-3546 (1993).
[28]R. H. Pry and C. P. Bean, J. Appl. Phys., 29(3), 532-533, (1958).
[29]S. V. Kulkarni and S. A. Khaparde, *Transformer Engineering: Design and Practice*, 1st ed. (Marcel Dekker, Inc., New York, 2004), p. 42.
[30]N. Stranges and R. D. Findlay, IEEE Trans. Magn., 36(5), 3457-3459(2000).
[31]H. Saadat, *Power system analysis*, 3rd ed. (PSA Publishing, U.S., 2010), p. 105.
[32]IEC 60404-6: 2018, *Magnetic materials - Part 6: Methods of measurement of the magnetic properties of magnetically soft metallic and powder materials at frequencies in the range 20 Hz to 100 kHz by the use of ring specimens*.
[33]JIS C 2553: 2019, *Cold-rolled grain-oriented electrical steel strip and sheet delivered in the fully processed state*, Japanese Industrial Standard.
[34]IEEE C57.163-2015, *IEEE Guide for Establishing Power Transformer Capability while under Geomagnetic Disturbances*.

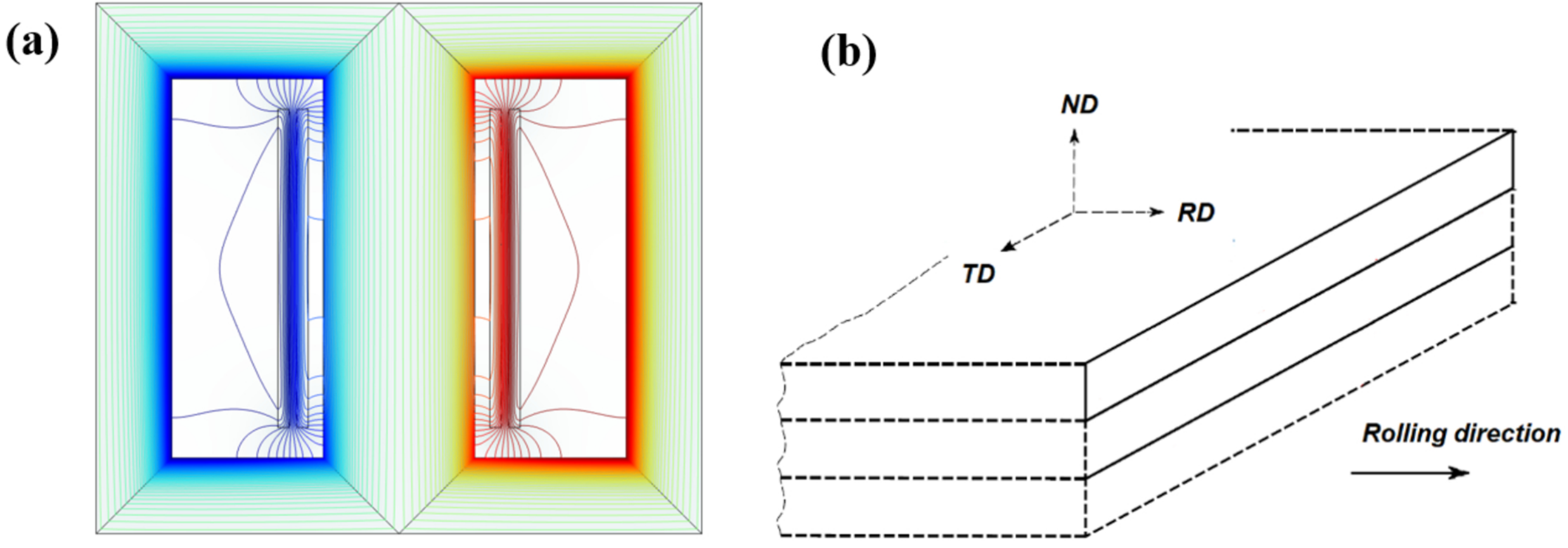
(a)
(b)
ND
RD
TD
Rolling direction

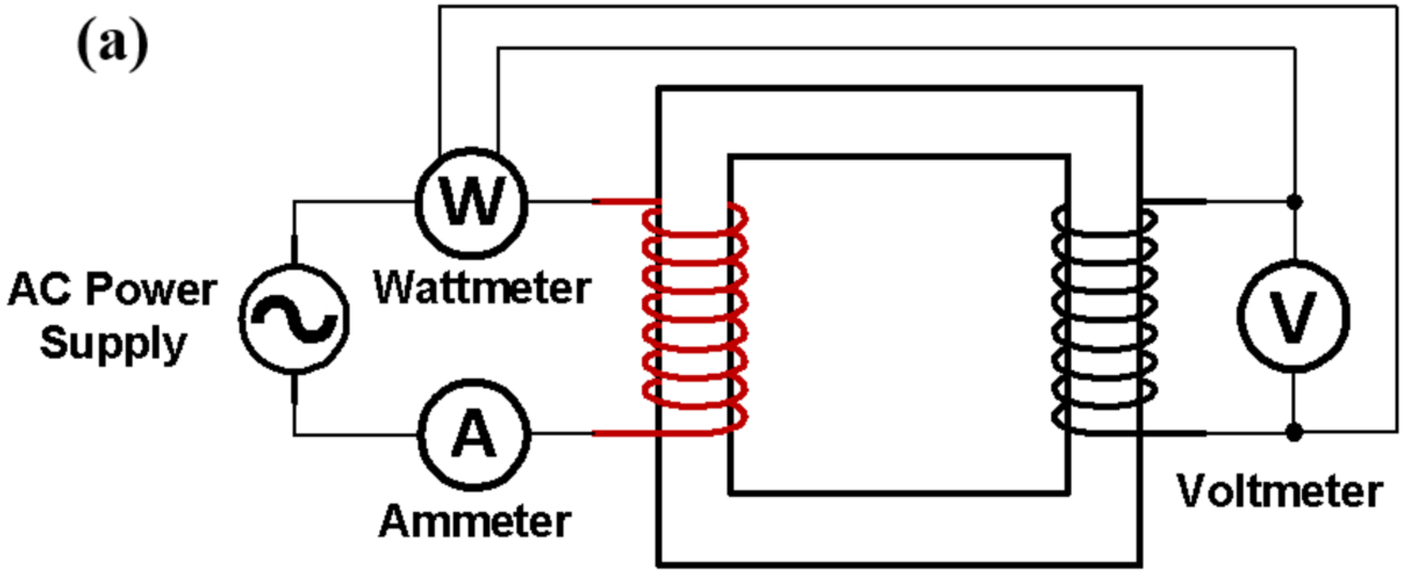
(a)
W
Wattmeter
AC Power
Supply
A
Ammeter
V
Voltmeter

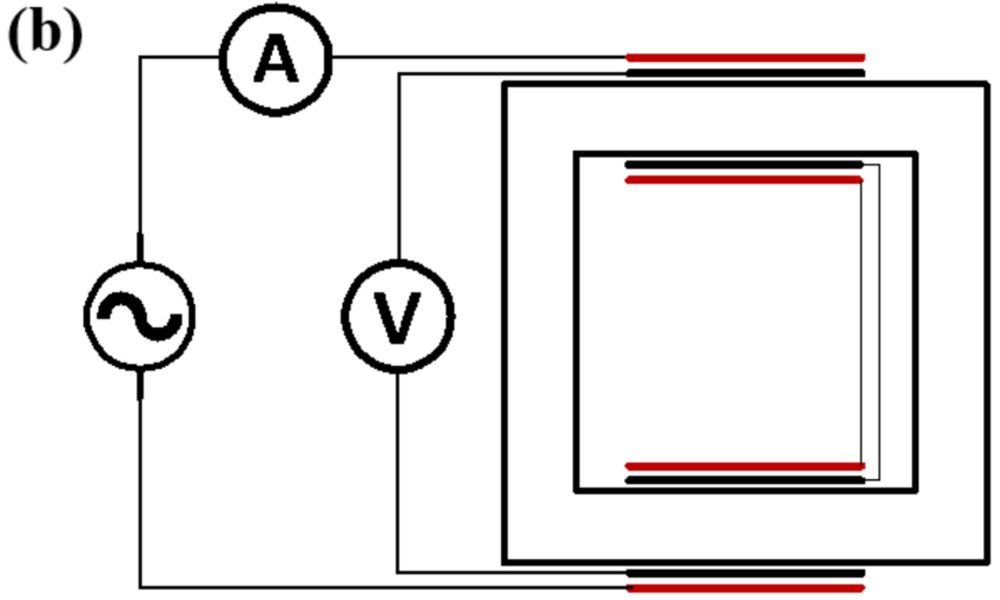
(b)
A
V

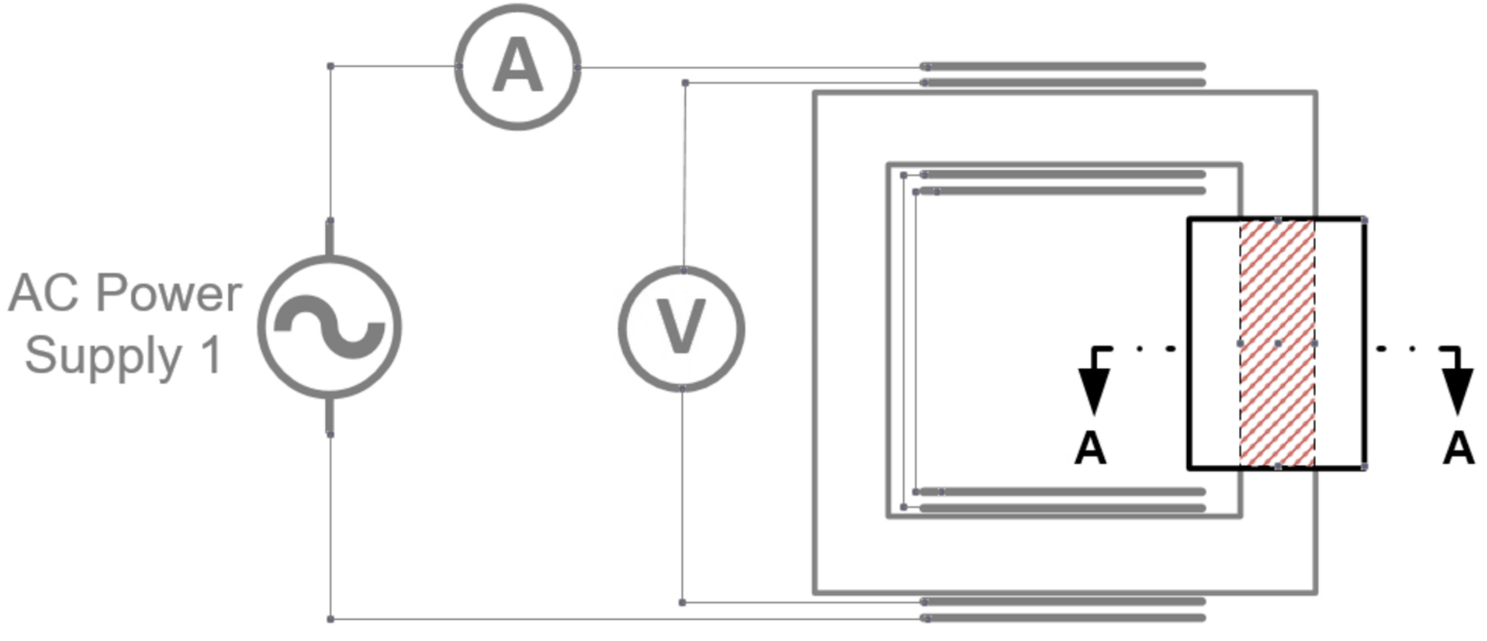
A
AC Power
Supply 1
V
A
A

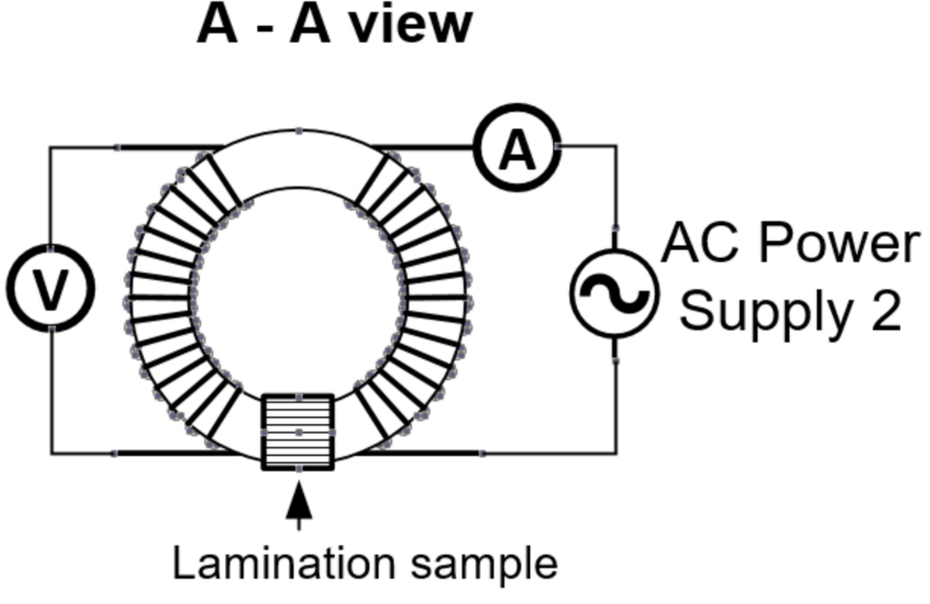
A - A view
A
V
AC Power
Supply 2
Lamination sample

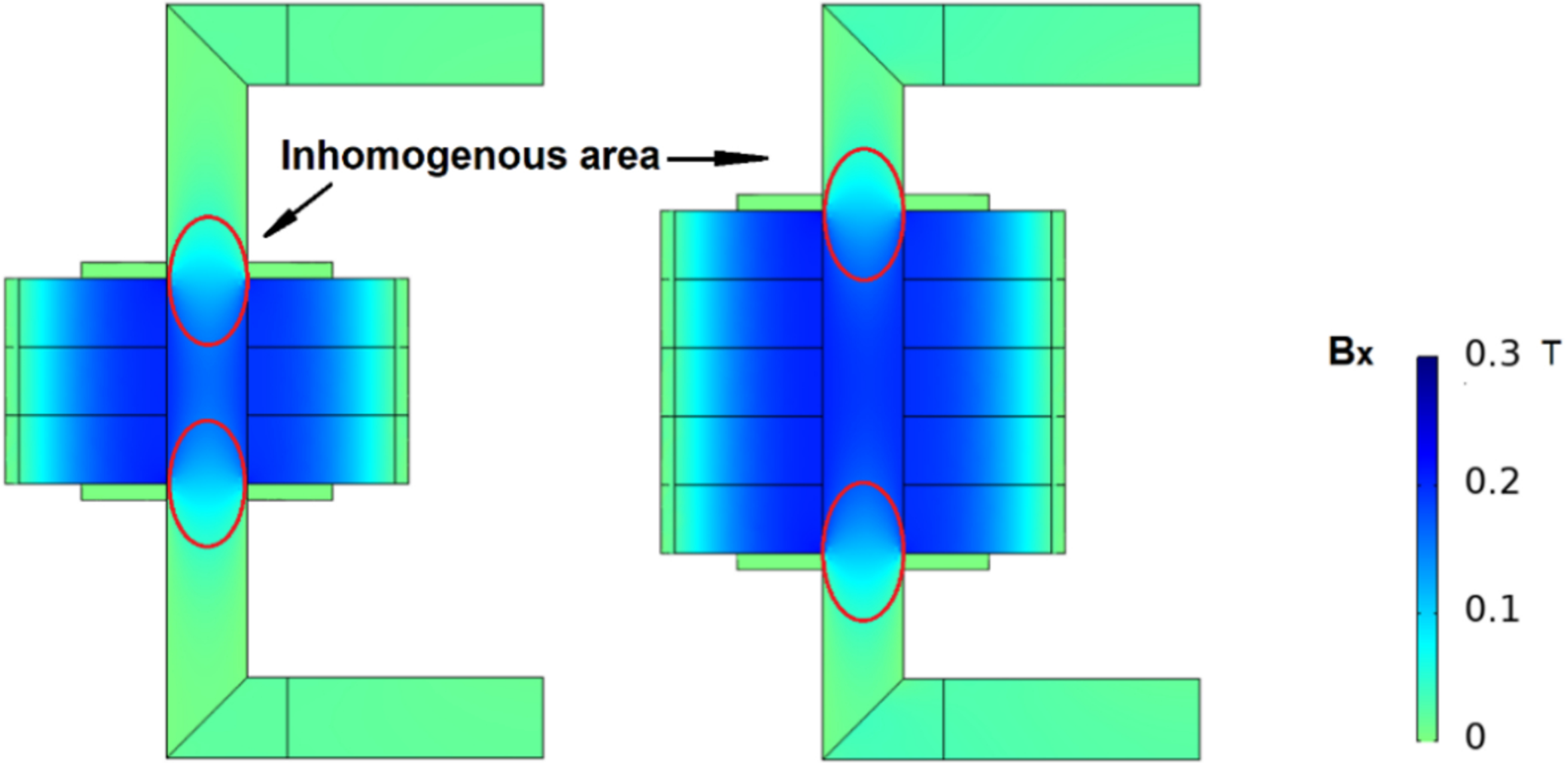
Inhomogenous area
Bx
0.3 T
0.2
0.1
0

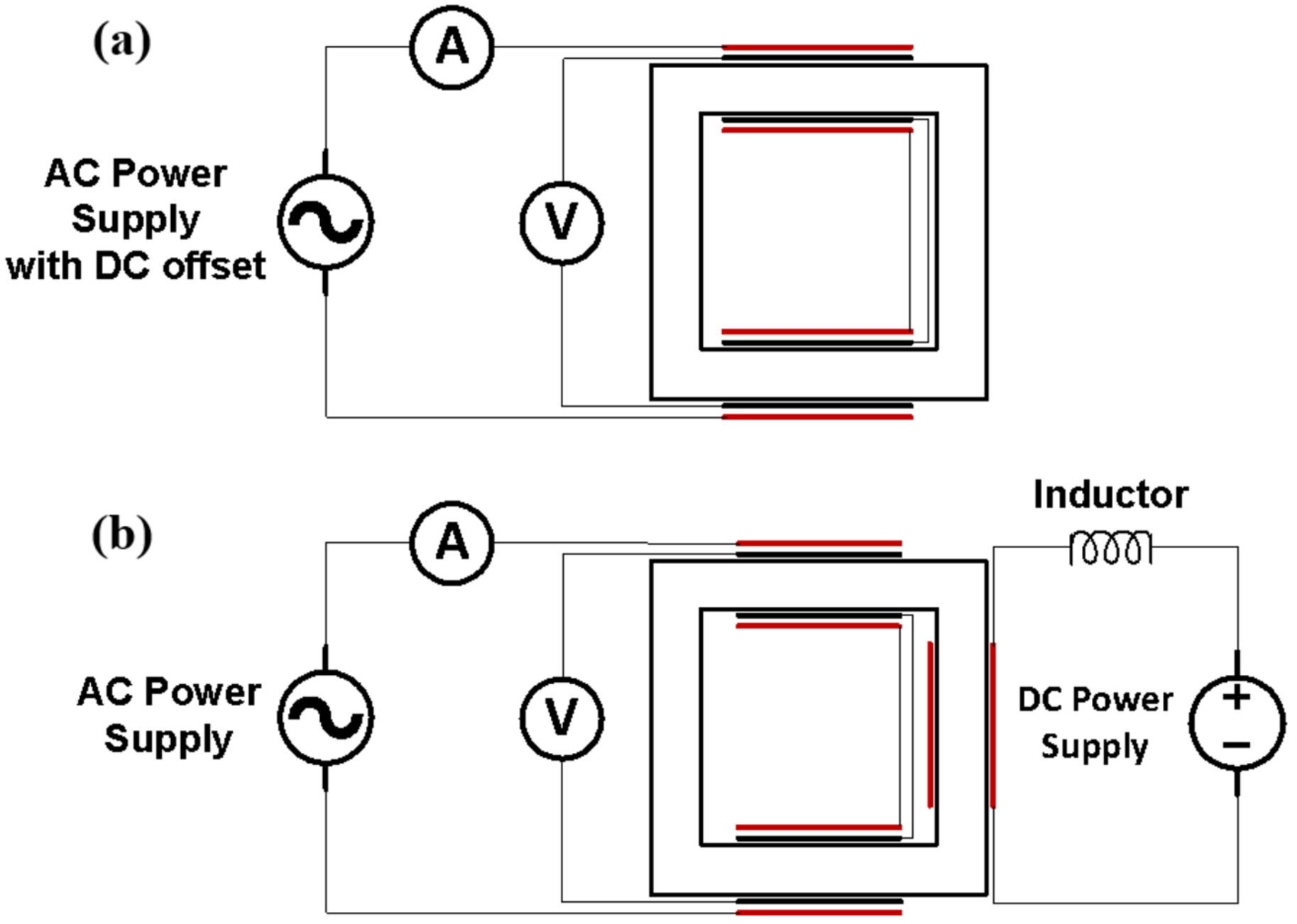
(a)
A
AC Power
Supply
with DC offset
V
(b)
Inductor
A
AC Power
Supply
V
DC Power
Supply
+
−

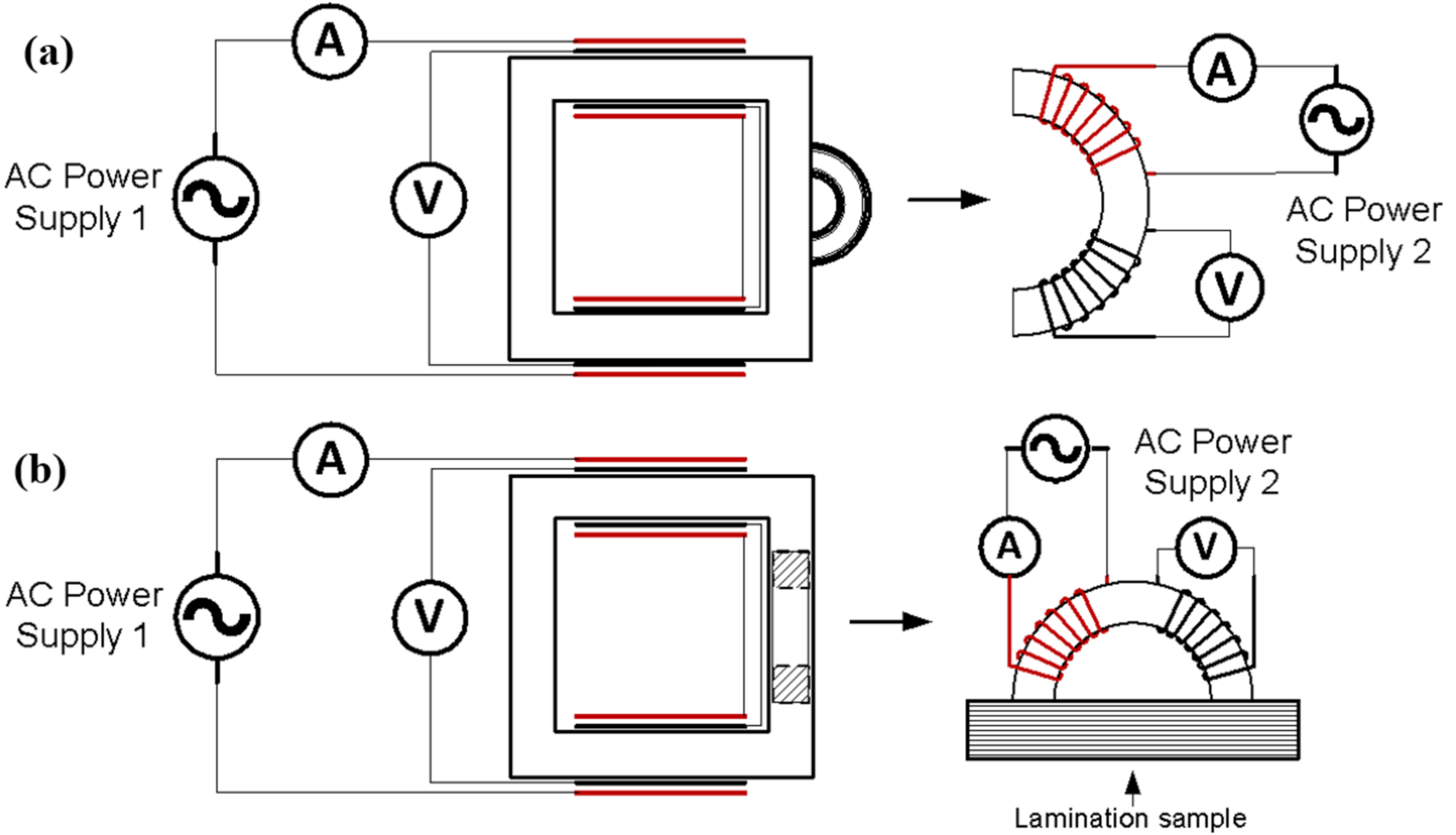
(a)
A
AC Power
Supply 1
V
A
AC Power
Supply 2
V
(b)
A
AC Power
Supply 1
V
AC Power
Supply 2
A
V
Lamination sample

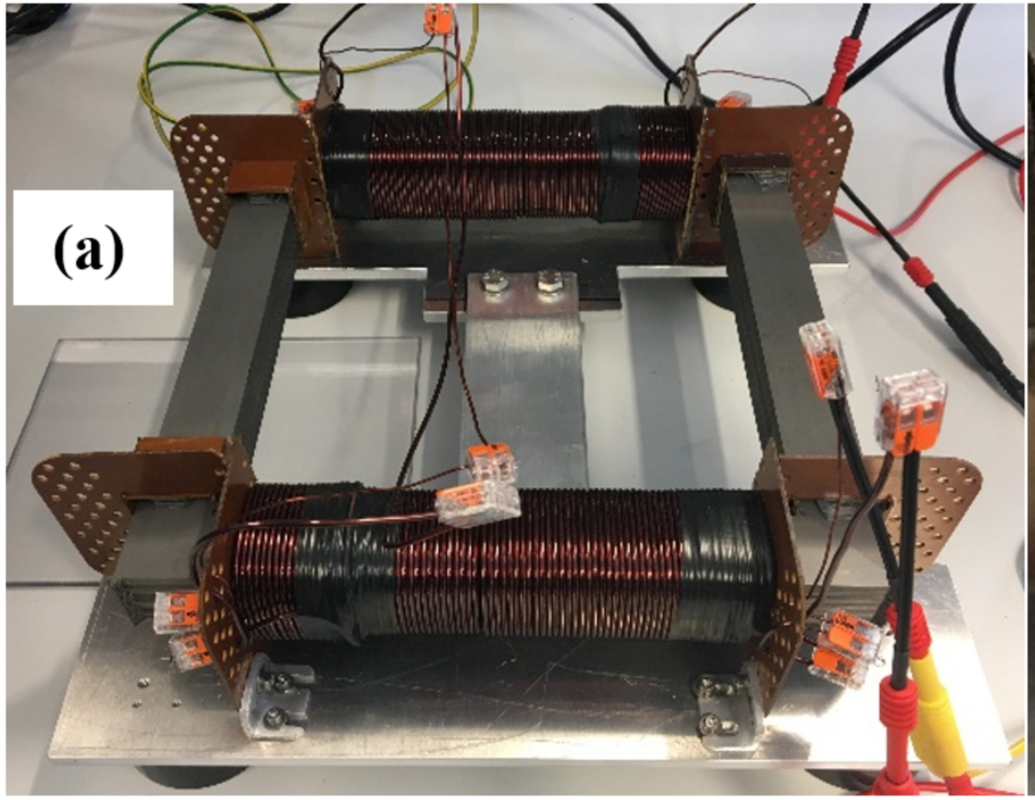
(a)

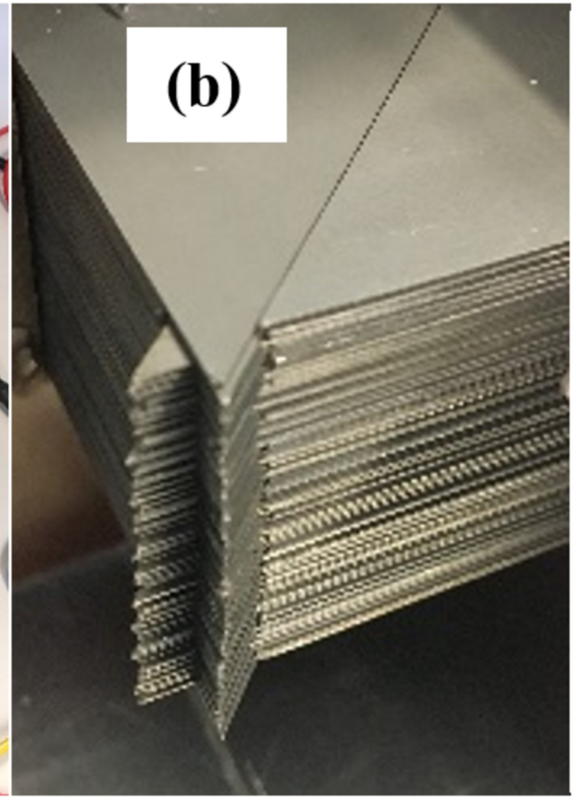
(b)

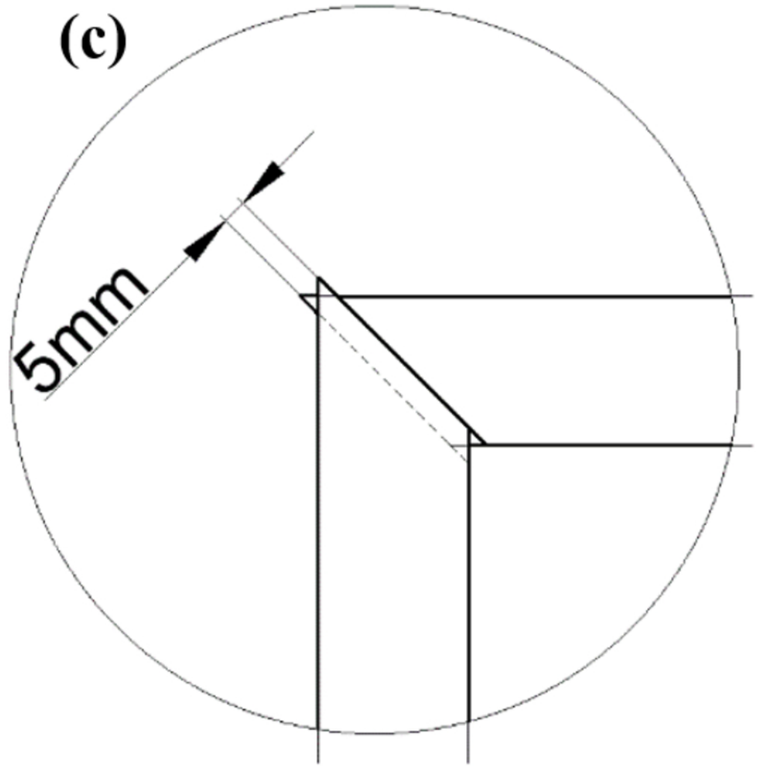
(c)
5mm

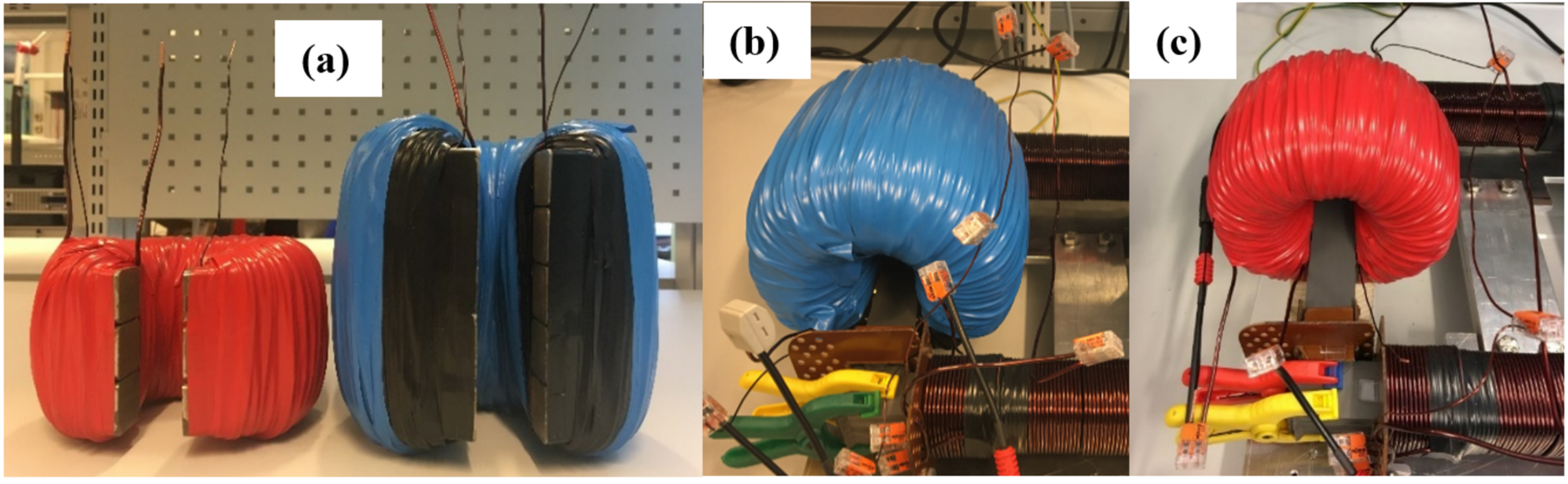
(a)
(b)
(c)

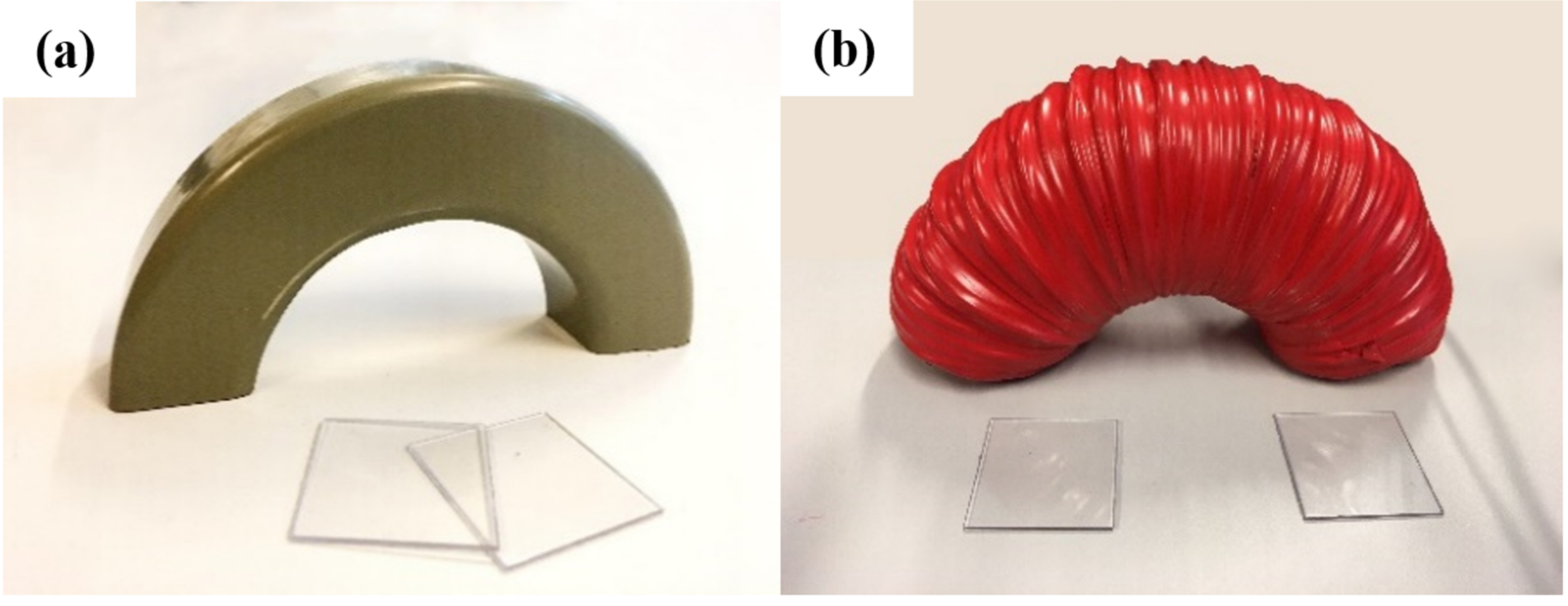
(a)
(b)

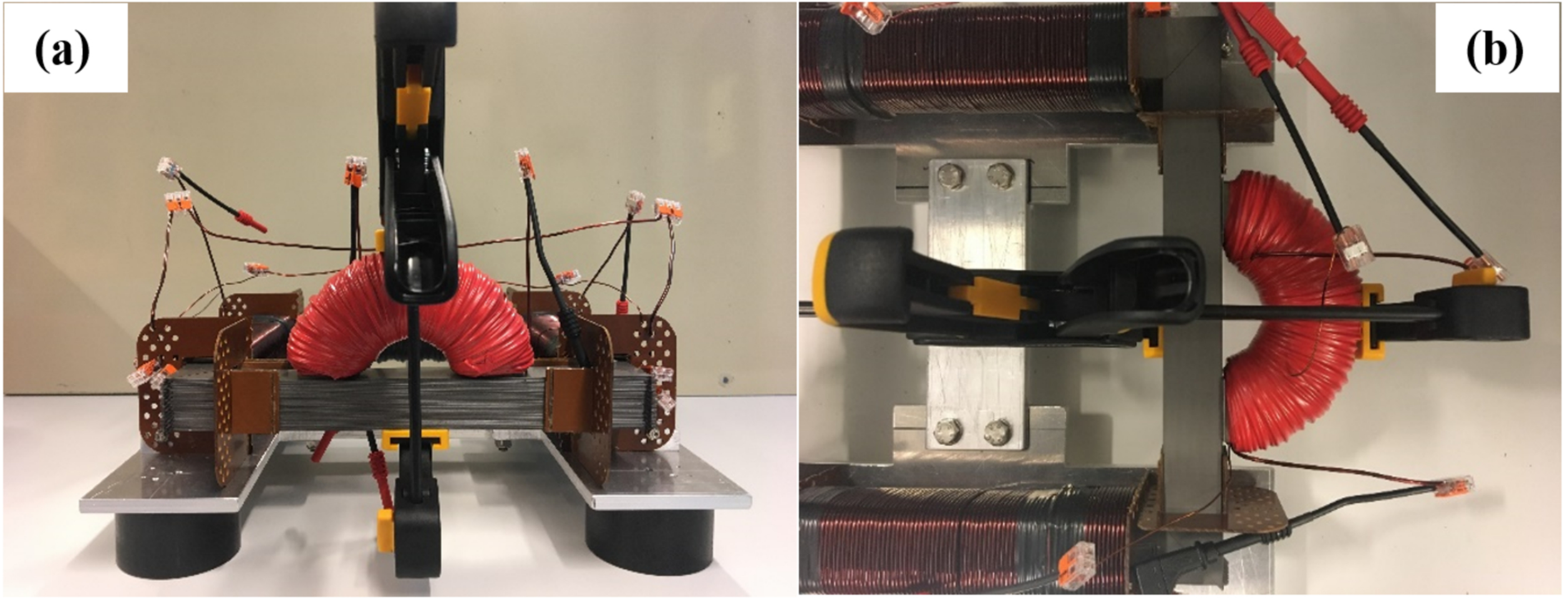
(a)
(b)

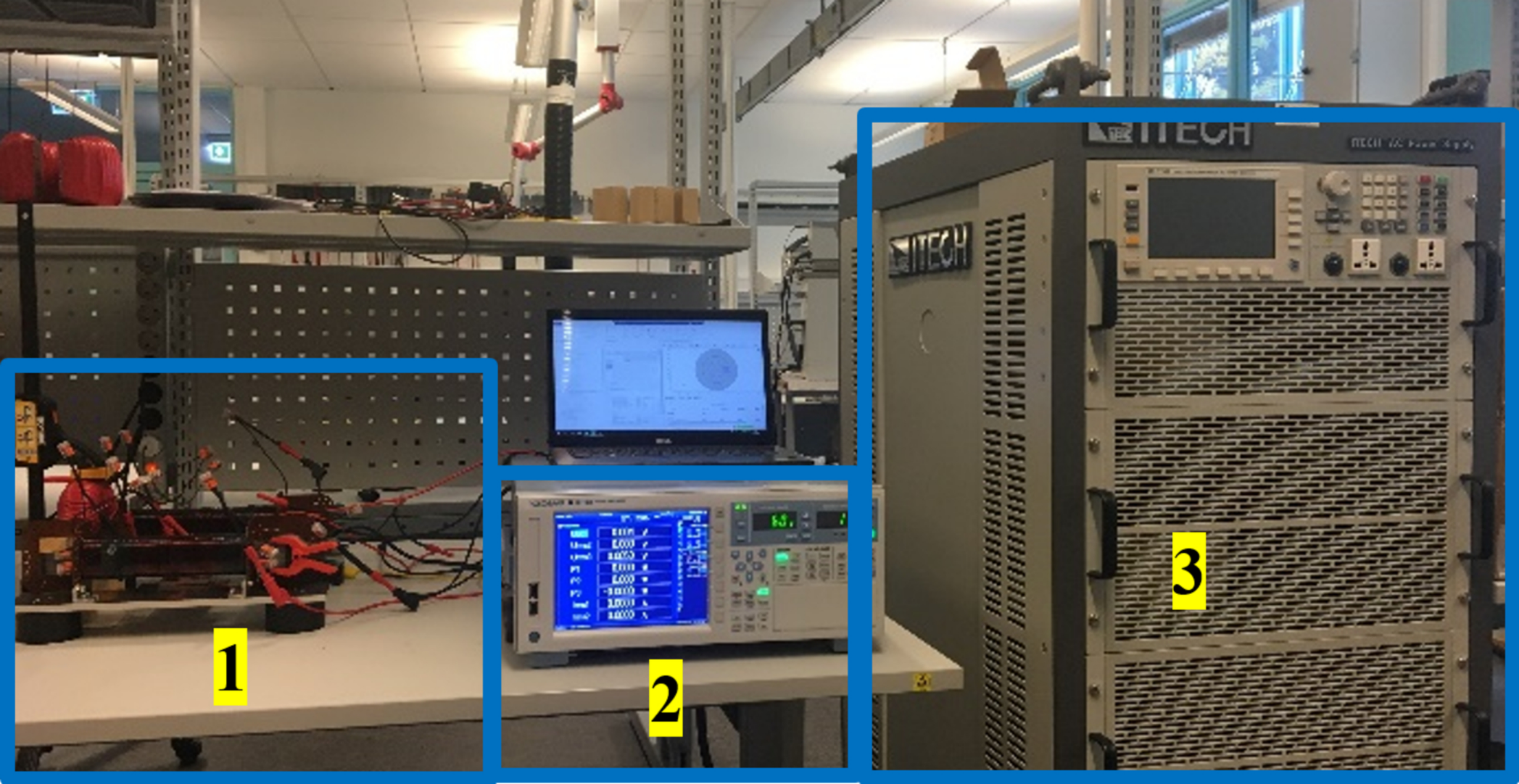
ITECH
1
2
3

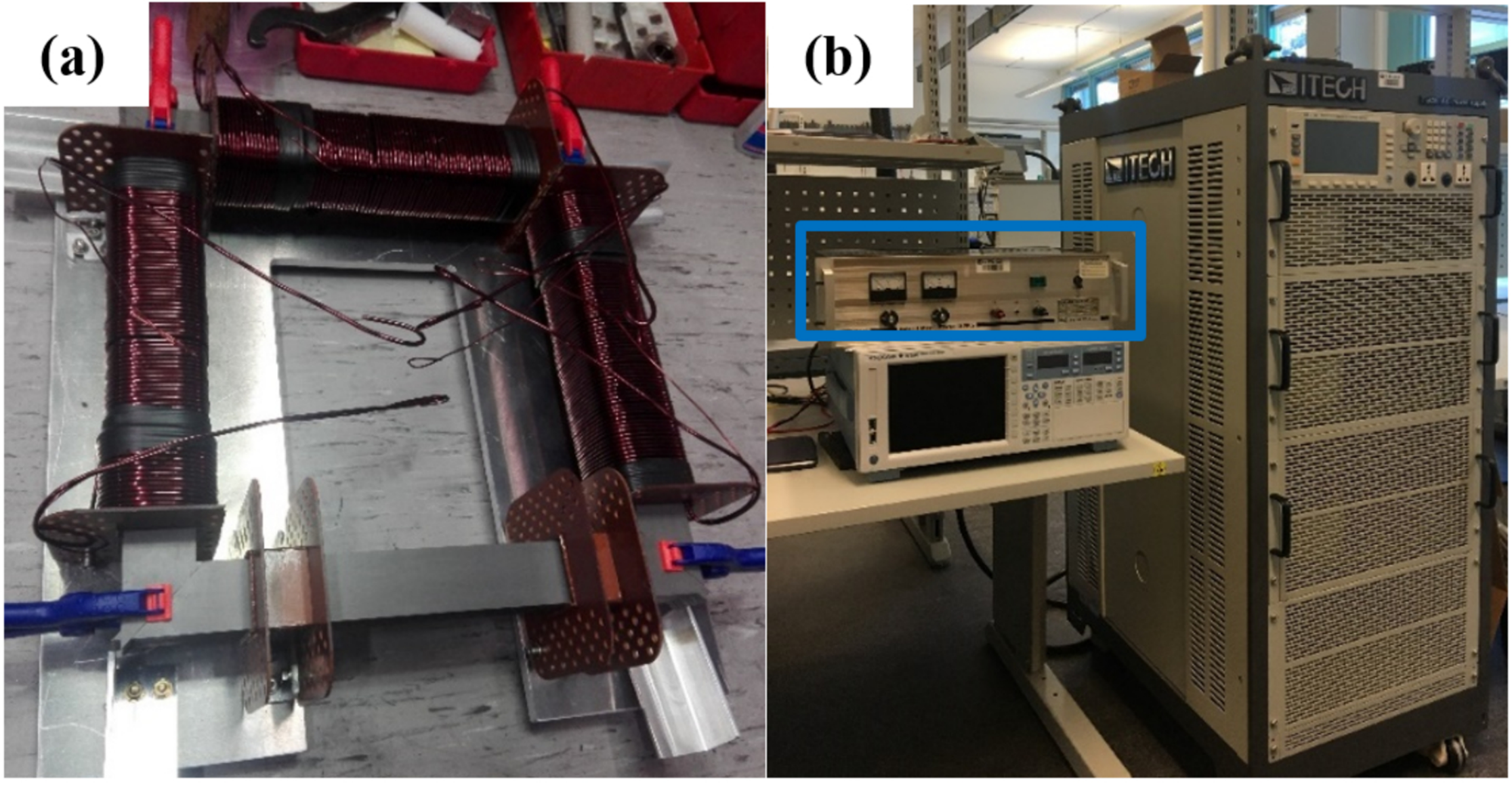
(a)
(b)
ITECH
ITECH

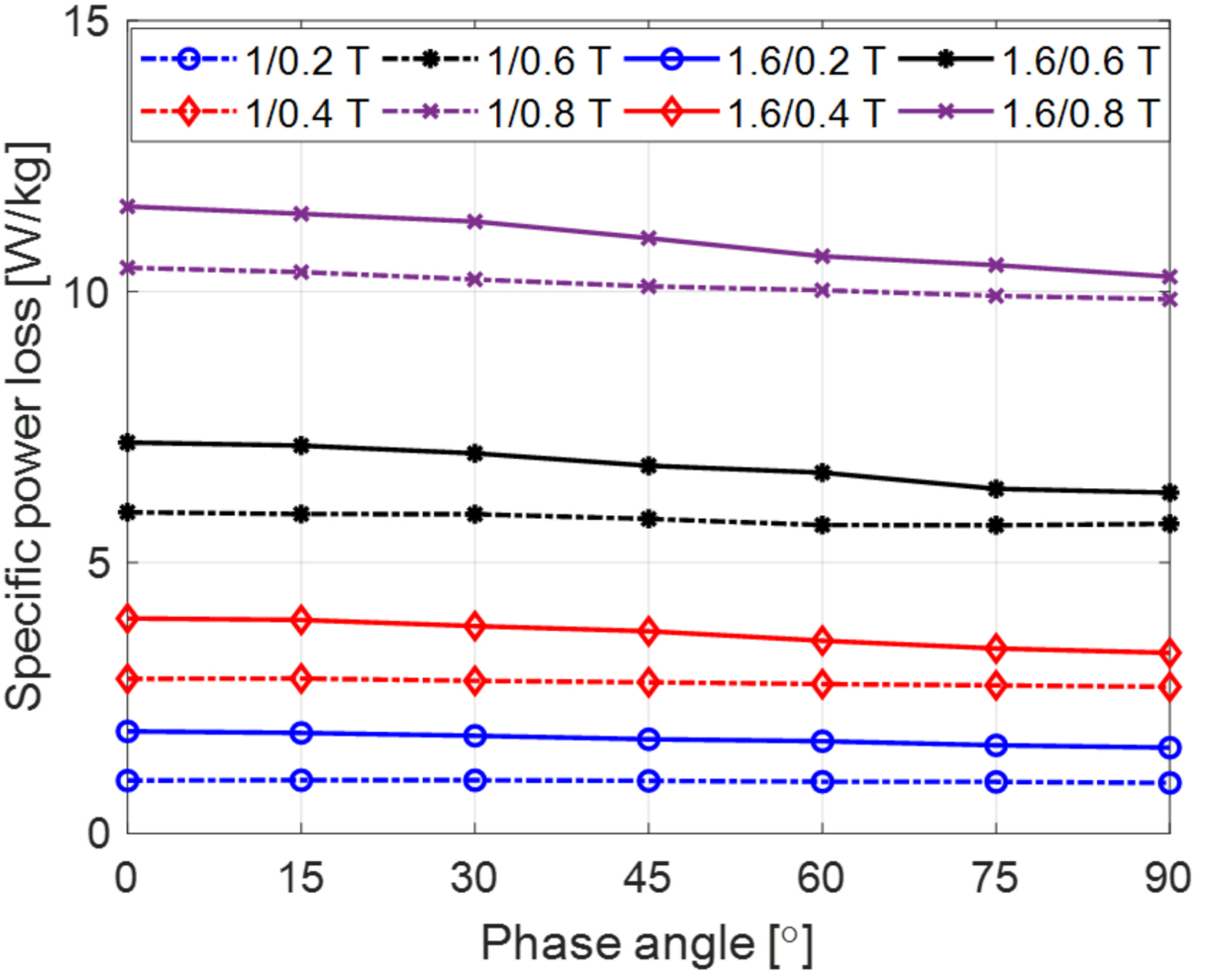
1/0.2 T
1/0.6 T
1.6/0.2 T
1.6/0.6 T
1/0.4 T
1/0.8 T
1.6/0.4 T
1.6/0.8 T
Specific power loss [W/kg]
Phase angle [°]
0
5
10
15
0
15
30
45
60
75
90

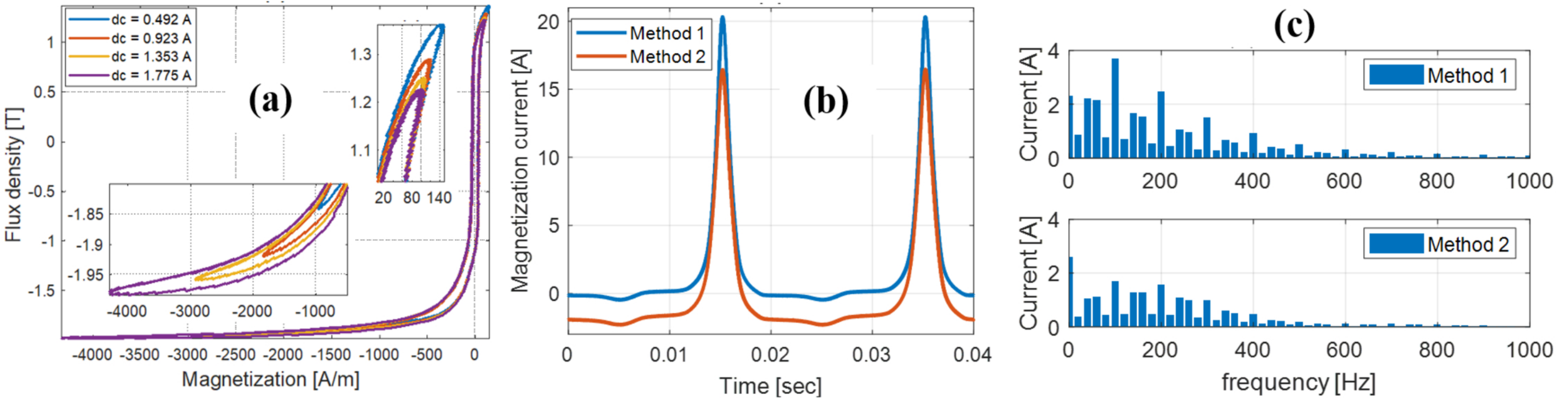
(a)
dc = 0.492 A
dc = 0.923 A
dc = 1.353 A
dc = 1.775 A
Flux density [T]
Magnetization [A/m]
(b)
Method 1
Method 2
Magnetization current [A]
Time [sec]
(c)
Method 1
Method 2
Current [A]
frequency [Hz]

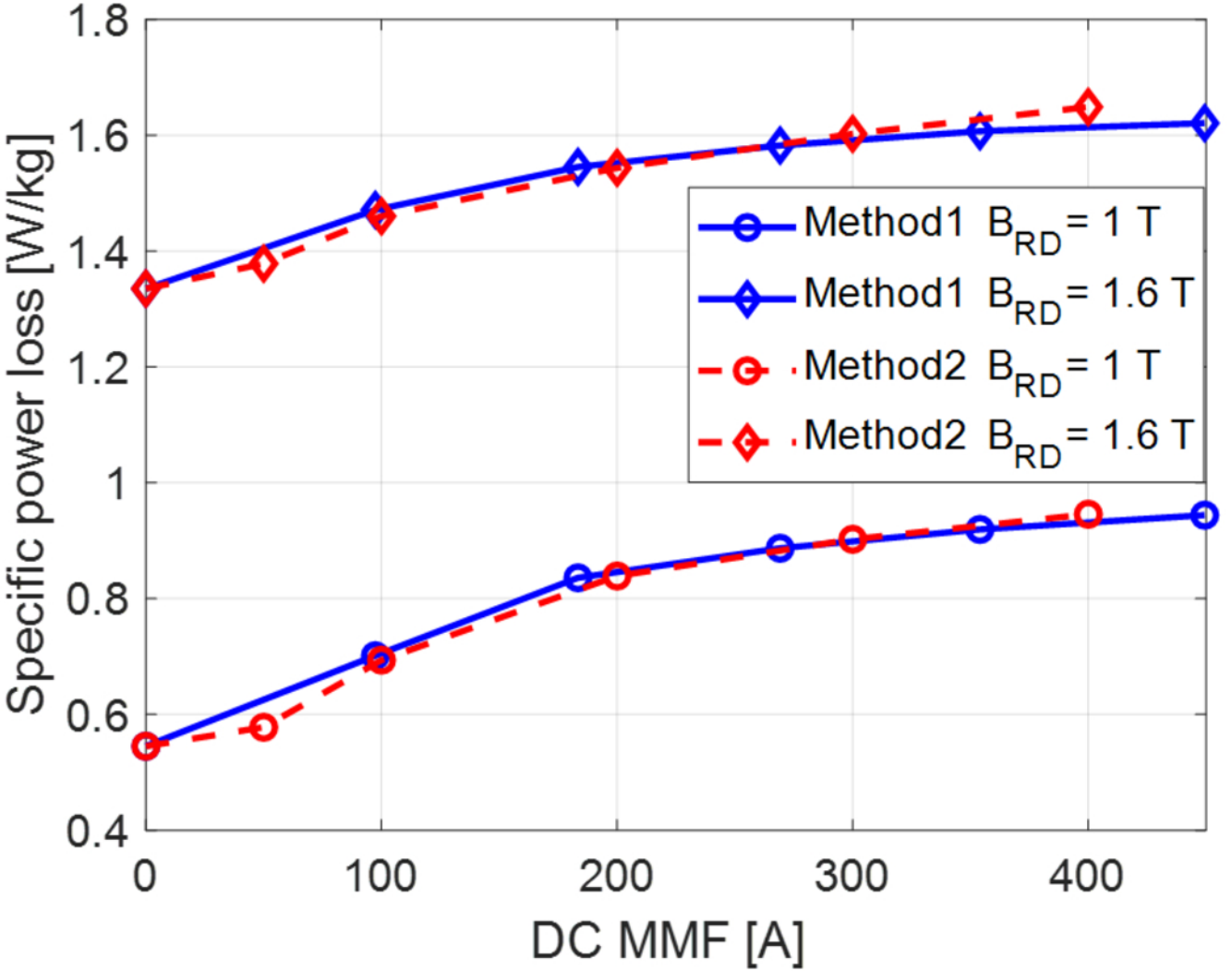
Specific power loss [W/kg]
DC MMF [A]
1.8
1.6
1.4
1.2
1
0.8
0.6
0.4
0
100
200
300
400
Method1 B_RD = 1 T
Method1 B_RD = 1.6 T
Method2 B_RD = 1 T
Method2 B_RD = 1.6 T

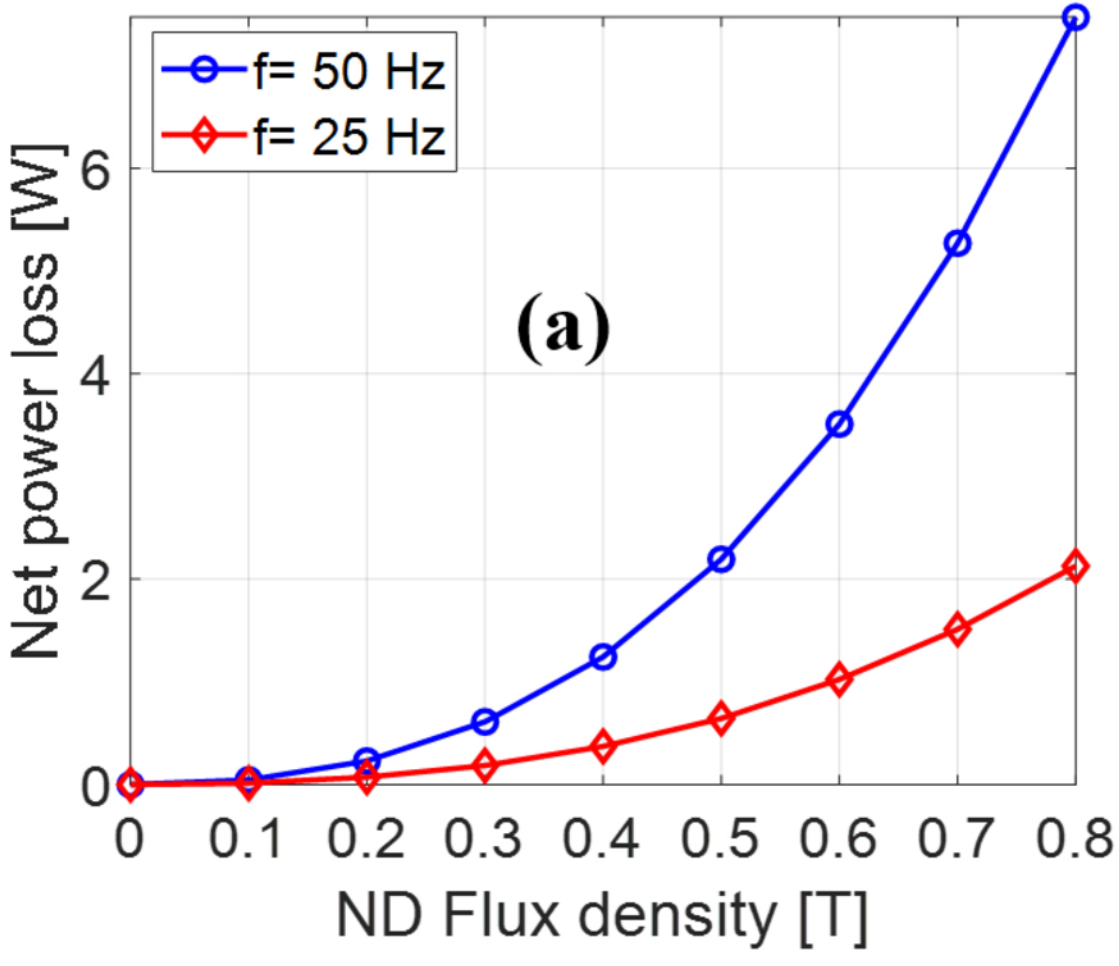
f= 50 Hz
f= 25 Hz
(a)
Net power loss [W]
ND Flux density [T]
0
2
4
6
0
0.1
0.2
0.3
0.4
0.5
0.6
0.7
0.8

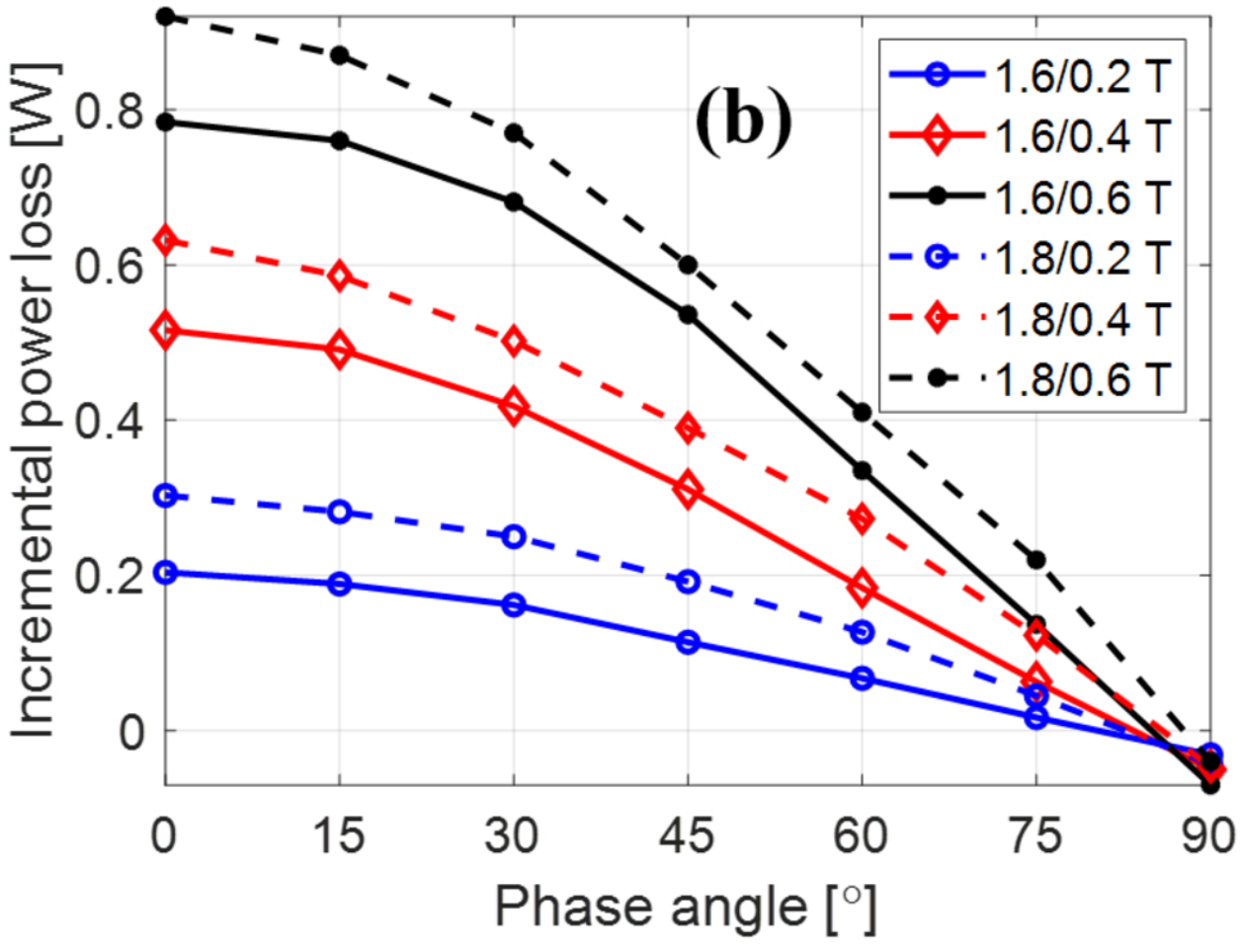
(b)
1.6/0.2 T
1.6/0.4 T
1.6/0.6 T
1.8/0.2 T
1.8/0.4 T
1.8/0.6 T
Incremental power loss [W]
Phase angle [°]
0
0.2
0.4
0.6
0.8
0
15
30
45
60
75
90